# Prolonged metaphase II arrest weakens Aurora B/C- dependent error correction in mouse oocytes

Antoine Langeoire[1,2,3], Alison Kem-Seng[2,3,4], Damien Cladière[1,2,3], Katja Wassmann[1,2,3*] and Eulalie Buffin[1,2,3*]

[1] Université Paris Cité, CNRS, Institut Jacques Monod, 75013 Paris, France

[2] Institut de Biologie Paris Seine, Sorbonne Université, 75252 Paris, France

[3] CNRS UMR7622, Developmental Biology Lab, Sorbonne Université, 75252 Paris, France

[4] Present address: Department of Biology, McGill University, Montréal, QC, Canada.

*: corresponding authors, eulalie.buffin@sorbonne-universite.fr, katja.wassmann@ijm.fr

**ABSTRACT**

Chromosome segregation during oocyte meiosis is highly error prone in mammals. Whereas control mechanisms at work during meiosis I have been studied quite extensively, our knowledge of these mechanisms in meiosis II is rather limited. The spindle assembly checkpoint (SAC) and error correction (EC) have to be adapted to the specificities of meiosis II, where attachments to the spindle are bipolar, and not monopolar. Additionally, errors occurring during meiosis I, are carried over into meiosis II. In this study we asked whether oocytes in meiosis II have the capacity to respond to attachments that are under less tension. We found that this was indeed the case, and Aurora B/C-dependent EC through SAC activation can mediate a metaphase delay. We also found that during the extended metaphase II arrest, necessary to await fertilization, spindle tension naturally decreases. However, this occurs concomitantly with a decrease in the sensitivity of EC due to an increase in PP2A at centromeres, with the result that only oocytes in early but not late metaphase II can respond to missing spindle tension.

## INTRODUCTION

The formation of haploid gametes, which is essential for sexual reproduction, requires two consecutive meiotic divisions, with no S-phase in between. First, homologous chromosomes are segregated in meiosis I, followed by meiosis II with the segregation of sister chromatids. Meiosis must be carried out precisely to produce embryos with the correct ploidy after fertilization. Aneuploidy in the embryo is mainly due to mis-segregation events in the oocyte and is the leading cause of miscarriage, infertility and birth defects in humans (Hassold & Hunt, 2001; Nagaoka & Hassold, 2013; Charalambous *et al*, 2023). Why female meiosis is highly error-prone is still a matter of debate, and possible explanations have been discussed in recent reviews (Kitajima, 2018; Mihajlovi & Fitzharris, 2018; Yakoubi & Wassmann, 2017; Charalambous *et al*, 2023).

Mammalian oocytes enter meiosis after premeiotic S-phase. During prophase I, homologous chromosomes recombine and are held together by the resulting chiasmata, forming a bivalent. Oocytes remain arrested in prophase I and only resume meiosis at sexual maturity following hormonal stimulation. Nuclear envelope breakdown, also known as GVBD (Germinal Vesicle Breakdown) is followed by the formation of a bipolar spindle. In mammalian oocytes, spindle assembly is a long process (4-6h in mouse) leading to the attachment of homologous chromosomes to the opposite poles of the spindle, with the sister kinetochores co-orienting to the same pole (Schuh & Ellenberg, 2007; Dumont & Desai, 2012). Chromosomes first attach laterally to microtubules, slide along the surface of the spindle towards the equator, and establish end-on microtubule attachments through the NDC80 complex located at kinetochores. Because initial attachments are often incorrect, they must be destabilized to give the microtubules a chance to re-attach correctly. Aurora B and the meiosis-specific Aurora C kinase are the enzymatic subunits of the Chromosomal Passenger Complex (CPC), which localizes at the centromere and interchromatid axis in meiosis I and promotes microtubule turnover at the kinetochore (Cairo *et al*, 2023; Avo Santos *et al*, 2011; Nguyen & Schindler, 2017; Balboula & Schindler, 2014; Tang *et al*, 2006). Thus, in meiosis I, bipolar attachments of homologous chromosomes are achieved after multiple rounds of Aurora B/C-dependent correction of faulty attachments (Kitajima *et al*, 2011; Kitajima, 2018).

In mitosis, it was shown that the kinetochore-microtubule (KT-MT) interaction is controlled by the phosphorylation state of the NDC80 subunit Hec1, which anchors the microtubule plus ends to the kinetochore. KT-MT interactions are destabilized by Aurora B phosphorylation of Hec1 and stabilized by PP2A-B56-mediated dephosphorylation of Hec1 (DeLuca *et al*, 2006, 2011; Welburn *et al*, 2010; Foley *et al*, 2011; Tang *et al*, 2016; Keating *et al*, 2020). The balance between Aurora B and PP2A-B56 activities is thought to depend on the tension that is generated between sister kinetochores when the opposing forces exerted by microtubules are in equilibrium. This spatial separation model proposes that the inter-kinetochore tension separates centromeric Aurora B from the kinetochore and reduces its ability to phosphorylate Hec1 and to destabilized KT-MT interaction. This model explains, at least in part, how Aurora B selectively destabilizes incorrect attachments, which are characterized by unbalanced pulling forces on sister kinetochores (Kitajima, 2018; McVey *et al*, 2021; Lampson & Cheeseman, 2011; Liu *et al*, 2009).

In meiosis I, since sister kinetochores are mono-oriented and pulled in the same direction, tension is not generated between the sister kinetochores as in mitosis or meiosis II, but between sister kinetochore pairs, and thus within kinetochores and across the entire bivalent chromosome. Even though this co-orientation of sister kinetochores may affect the tension-sensing mechanism, reducing tension in metaphase I induces Hec1 phosphorylation by Aurora B/C, and Spindle Assembly Checkpoint (SAC) activation as a consequence of microtubule detachment, as we have shown previously in mouse oocytes (Vallot *et al*, 2018). But Aurora B/C persists in the vicinity of kinetochores even after biorientation and bivalent stretching, potentially preventing attachment stabilization. It has been proposed that attachment stabilization is mainly mediated by the progressive accumulation of PP2A-B56 phosphatase at kinetochores during meiosis I (Yoshida *et al*, 2015).

After homologous chromosome segregation in anaphase I, followed by first polar body extrusion, oocytes immediately enter meiosis II without entering S-phase. The transition from meiosis I to meiosis II, called interkinesis, is characterized by partial chromosome decondensation and the absence of a bipolar spindle. After interkinesis, spindle assembly in mouse oocyte meiosis II takes place within 1 hour, and is thus strikingly faster than in meiosis I (Kouznetsova *et al*, 2019; Dumont *et al*, 2007). In vertebrate oocytes, including mammals, meiosis arrests again at metaphase II, with sister chromatids attached in a bipolar fashion, in contrast to meiosis I (Petronczki *et al*, 2003). This cell cycle arrest, maintained by

CSF (Cytostatic Factor) activity, persists until fertilization takes place. Sperm entry triggers sister chromatid segregation, second polar body extrusion, and eventually zygote formation upon fertilization (Ozturk, 2022). Since mammalian oocytes are arrested in metaphase II until fertilization, they should have more time to correct faulty chromosome attachments. However, 20% of chromosomes are misaligned in mouse metaphase II arrested oocytes, suggesting that some incorrect attachments are not detected and thus, not corrected in meiosis II (Kouznetsova *et al*, 2019). In addition, meiosis II has to deal with segregation errors carried over from meiosis I. In this respect, it is important to note that in mouse oocytes, single sister chromatids resulting from precocious separation in meiosis I are not efficiently recognized in meiosis II and escape error correction and SAC activation (Kouznetsova *et al*, 2014). Therefore, it is essential to better understand how correct attachments are achieved during meiosis II, and why errors occur.

Here, to investigate the efficiency of the error correction pathway in meiosis II, we asked whether tension-less attachments can be detected and corrected in meiosis II. Unexpectedly, we found that after prolonged arrest in metaphase II, the inter-kinetochore (inter-KT) tension is naturally reduced while chromosomes are correctly bioriented and aligned. Further reducing tension at this time does not promote Aurora B/C-dependent microtubule detachment, or SAC activation, in contrast to reducing tension at an earlier stage. We conclude that when oocytes are kept arrested in metaphase II to await fertilization, attachments, even incorrect ones, are stabilized by PP2A-B56 accumulating at the kinetochore and counteracting Aurora B/C, regardless of the level of tension. This may explain the persistence of misaligned chromosomes in metaphase II oocytes, eventually contributing to high aneuploidy rates.

## RESULTS

### Chromosomes continue to align correctly in metaphase II

First, to define when oocytes are in metaphase II, we characterized spindle reformation and chromosome alignment after anaphase I by time-lapse microscopy in mouse oocytes expressing H2B-RFP and Tubulin-GFP (Fig1A-B). In our strain background, chromosomes segregate in anaphase I approximately 7 h after GVBD. After polar body extrusion,

chromosomes appear partially decondensed but remain close together, even though the spindle did not reassemble yet. This transition phase (interkinesis) lasts for about 1 h. Then, chromosomes condense again, begin to individualize, and the metaphase II spindle assembles rapidly, mainly by nucleating microtubules from the chromosomes. Chromosomes start to align at the equator around 10 h after GVBD. Visualization of a metaphase plate defines the transition from prometaphase II to metaphase II, even though chromosomes continue to oscillate throughout the metaphase II arrest (Fig1A-B, Movie1).

To determine more precisely when chromosome alignment is achieved, we quantified the number of unaligned chromosomes in fixed oocytes at different times in meiosis II (Fig1C-D). We observed that the percentage of oocytes containing unaligned chromosomes decreases with time from 75% at 12 h to 11% at 18 h after GVBD. As our protocol included a short cold treatment to remove unstable microtubules prior to spindle fixation, we confirmed that the same percentage of unaligned chromosomes was observed without cold treatment (FigS1A-B). This is consistent with previous results, which reported that incorrect attachments persist until metaphase II arrest (Kouznetsova *et al*, 2019). In this study, oocytes are considered to be in metaphase II around 2.5 h after anaphase I when the equatorial plate become visible. Accordingly, and based on our observations, we considered that oocytes at 12 h after GVBD (5 h after anaphase I) are in early metaphase II, with most but not all chromosomes aligned at the metaphase plate. On the other hand, we considered oocytes as arrested in late metaphase II at 18 h after GVBD (11 h after anaphase I) when better alignment was achieved, as indicated by the reduction in metaphase plate width (FigS1C-D).

**Proper chromosome alignment does not correlate with high tension in late metaphase II**

Chromosome alignment depends on attachment status (correct (bipolar) or incorrect, such as monopolar or merotelic) as well as balance of forces exerted by microtubules on each sister kinetochore. We therefore expected that chromosome alignment would correlate with increased tension between sister kinetochores. Indeed, it has already been observed that inter-KT distance, a measure commonly used to estimate the tension applied on sister kinetochore pairs, increased from prometaphase II to early metaphase II (Kouznetsova *et al*, 2019). Surprisingly, we observed here that once oocytes are in metaphase II, the inter-KT distance progressively decreased from 2.3 µm at 12 h to 1.4 µm at 18 h after GVBD instead

of increasing as expected (Fig1E-F). In other words, in oocytes arrested in late metaphase II and awaiting fertilization, attachments are naturally under less tension than in early metaphase II oocytes.

The striking reduction of tension in late metaphase II has not been described before and could be explained, at least in part, by increased spindle stability. Indeed, we have shown that the spindle becomes more resistant to depolymerization by cold treatment at 18 h after GVBD compared to 12 h (FigS1E-F). Since microtubule dynamics contribute to the pulling forces exerted on kinetochores, increased microtubule stability would reduce inter-KT tension similar to what has been observed upon hyperstabilization of spindles in mitosis by taxol treatment (Maresca & Salmon, 2009; Ye *et al*, 2016). This observation however raises the question of how incorrect attachments may get recognized and selectively destabilized if correct attachments also lack tension in late metaphase II.

**The SAC is functional throughout metaphase II**

We have shown that inter-KT tension naturally decreases in late metaphase II, even though most chromosomes are correctly bioriented and aligned. Thus, these tension-less attachments should not be corrected to allow proper completion of meiosis II upon fertilization. Consequently, the SAC or the CPC should be turned off in late metaphase II to prevent oocytes from recognizing tension-less attachments as incorrect and thus destabilizing even correct attachments. However, the SAC and the CPC need to be active in early metaphase II, when unaligned chromosomes are still present, to allow their correction.

Therefore, we first asked whether the SAC remains functional in late metaphase II and whether it is able to block anaphase II onset upon nocodazole-induced missing attachments. To assess SAC activity, we monitored APC/C-dependent degradation of exogenously expressed Securin-YFP. *In vivo*, anaphase II is induced by fertilization, which can be mimicked *in vitro*, by activating oocytes with strontium treatment (Fig2A). In the absence of nocodazole, Securin-YFP was degraded, whereas this was not the case after addition of nocodazole either in early or late metaphase II, showing that the SAC is functional and can be activated efficiently upon gross loss of kinetochore attachments (Fig2B; FigS2A-B; Movies 2 and 3). Accordingly, the SAC protein Mad2, which was almost completely absent from kinetochores in control oocytes, was recruited to unattached kinetochores after

depolymerization of microtubules with nocodazole in both early and late metaphase II, indicating that the SAC is well functional at both time points (Fig2C-D). This result shows that the SAC retains its functionality in late metaphase II and could theoretically be activated if tension-less attachments are released by the destabilizing activity of Aurora B/C.

**Low tension in early metaphase II induces SAC activation in an Aurora B/C-dependent way**

Since the SAC is functional in early and late metaphase II, we hypothesized that the tension-sensing mechanism itself is inefficient to sense and thus correct tension-less attachments in late metaphase II. But turning off the tension-sensing mechanism too early runs the risk of leaving some errors uncorrected. Therefore, we tested first CPC functionality in early metaphase II, when some unaligned chromosomes persist. STLC, an inhibitor of the kinesin Eg5, was used to provoke tension-less attachments in early metaphase II (Skoufias *et al*, 2006). By promoting the pole-separating forces required for spindle bipolarization, Eg5 contributes to the pulling forces on kinetochores (Schuh & Ellenberg, 2007; Mailhes *et al*, 2004). In meiosis I, Eg5 inhibition by STLC induced shorter spindles and reduced chromosome bivalent stretching between pairs of sister kinetochores (Vallot *et al*, 2018). As expected, also in meiosis II, STLC reduced spindle length and inter-KT distance in early metaphase II, confirming the efficiency of Eg5 inhibition (FigS3A-B).

To investigate whether low tension can induce microtubule detachment by the CPC, we asked whether anaphase onset is delayed as a result of SAC activation. Timing of anaphase onset was determined by following sister chromatid segregation in H2B-RFP-expressing oocytes by live imaging (Fig2A). When control oocytes were activated with strontium in early metaphase II (12 h after GVBD), 50% of oocytes segregated sister chromatids within 2 h after strontium addition (Fig2E, G - dotted red curve). Crucially, when STLC was added in early metaphase II, anaphase II was strongly delayed: only 30% of STLC-treated oocytes segregated sister chromatids within 5 h after addition of strontium (Fig2E, G - solid red curve; FigS2C; Movie 4). Accordingly, the SAC protein Mad2 was recruited to kinetochores when oocytes were treated with STLC, confirming that the SAC is activated upon reduced tension (Fig2C-D). Moreover, after inhibition of the essential SAC protein Mps1 with the drug reversine, STLC-treated oocytes were now able to enter anaphase II after strontium addition, due to override of the SAC. Sister chromatids segregated even earlier than in control

oocytes, supporting that the SAC is still active and is delaying cell cycle progression in early metaphase II control oocytes (Fig2E - solid grey curve; FigS2C; Movie 4). Thus, the SAC is well activated after inducing low tension in early metaphase II, suggesting that tension-less attachments can be detected and destabilized in early metaphase II.

Next, we asked whether the anaphase delay observed after artificially reducing tension in early metaphase II, requires CPC activity. In STLC-treated oocytes, Securin-YFP degradation was delayed compared to control oocytes (Fig2F - red curves; Fig S3D). After inhibition of Aurora B/C with AZD1152, STLC-treated oocytes were able to degrade Securin-YFP without delay, indicating APC/C activation and SAC satisfaction in early metaphase II (Fig2F - dotted grey curve; FigS3D, Movie 5). Of note, in this last experiment, we chose to follow Securin-YFP degradation as an indicator of anaphase onset, because Aurora B/C inhibition perturbs sister chromatid segregation, making anaphase II onset more difficult to visualize. Thus, artificially reducing tension in early metaphase II prevents anaphase II from occurring only when Aurora B/C is active. This suggests that tension-less attachments promote Aurora B/C-dependent error correction. As a result, the SAC is activated and blocks anaphase II onset, similar to meiosis I, as we have shown previously (Vallot *et al*, 2018).

**Low tension in late metaphase II does not induce SAC activation**

We have shown that in early metaphase II, artificial reduction of tension can be detected efficiently by Aurora B/C and can induce a SAC-dependent delay of anaphase II onset. However, we also found that inter-KT tension naturally decreases in late metaphase II when chromosomes are correctly aligned. This implies that attachments under low tension in late metaphase II should not be recognized as incorrect attachments, otherwise they would be destabilized. Thus, we hypothesized that error correction is turned off in late metaphase II to preserve correct attachments.

To address this issue, we treated oocytes in late metaphase II with STLC to determine whether low tension induces a SAC-dependent anaphase II delay after activation with strontium (Fig2A). As expected, STLC reduced spindle length in late metaphase II oocytes, confirming the efficiency of Eg5 inhibition (FigS3C). However, because tension was already low in late metaphase II, STLC does not further reduce inter-KT distance (FigS3D). To assess error correction in late metaphase II under the same experimental conditions as before in

early metaphase II, we compared untreated late metaphase II oocytes with natural low tension, with oocytes at the same cell cycle stage treated with STLC. When STLC was added in late metaphase II, 50% of oocytes segregated sister chromatids 40-50 min after strontium addition, similar to untreated control oocytes activated in late metaphase II (Fig2G - blue curves; FigS3E; Movie6). Anaphase II is therefore induced rapidly, even after STLC treatment in late metaphase II oocytes. Thus, tension-less attachments do not promote SAC activation in late metaphase II. Accordingly, the SAC protein Mad2 remained at low levels on most kinetochores when oocytes were treated with STLC in late metaphase II (Fig2C-D).

Our results indicate that even though the SAC is functional in early and late metaphase II, it is not activated in late metaphase II, when inter-KT tension is physiologically low. Artificially decreasing tension in early metaphase II leads to a SAC dependent delay, but has no effect in late metaphase II. Our results suggest that there is a temporal window during which low tension can be detected and induce SAC activation. This window coincides with the presence of a significant number of unaligned chromosomes in early metaphase II. In late metaphase II, when most chromosomes are correctly aligned, naturally occurring low tension is tolerated and becomes thus unable to activate the SAC.

**Aurora B/C-dependent error correction in late metaphase II is not efficient enough to promote microtubule detachment**

Artificial low tension in early metaphase II can induce SAC activation but natural low tension in metaphase II cannot, suggesting that Aurora B/C-dependent error correction is efficient enough to promote microtubule detachment in early metaphase II but not in late metaphase II. To confirm when tension-less attachments promote destabilization of KT-MT interactions in metaphase II, we investigated whether adding STLC affected Aurora B/C-dependent phosphorylation of Hec1 on Serine 55, which serves as a read-out of MT destabilization and ongoing error correction in mitosis (DeLuca *et al*, 2011). The level of Hec1 phosphorylation was similar in early and late metaphase II control oocytes, suggesting that most attachments are already stabilized in early metaphase II, although some unaligned chromosomes persist (Fig3A-B). It is reasonable to assume that unaligned chromosomes show higher Hec1 phosphorylation, however, we did not compare Hec1 phosphorylation between aligned and unaligned chromosomes here. Crucially, treating oocytes with STLC in early metaphase II

increased Hec1 phosphorylation much more than in late metaphase II (Fig3A-B). This result confirms that tension-less attachments are indeed destabilized in early metaphase II, consistent with the observed SAC activation and anaphase delay. In contrast, tension-less attachments in late metaphase II are not sufficiently destabilized to activate the SAC.

**Higher PP2A levels at kinetochores stabilize tension-less attachments in late metaphase II**

The level of Hec1 phosphorylation results from the balance between Aurora B/C kinase and PP2A-B56 phosphatase activities. The overall failure to phosphorylate Hec1 on Serine 55 in late metaphase II may be due to a shift in the balance towards more PP2A-B56, compared to early metaphase II. More PP2A-B56 activity may counteract Aurora B/C-dependent phosphorylation of Hec1 in late metaphase II, as already shown in meiosis I (Yoshida *et al*, 2015). Hence, we compared PP2A levels in early and late metaphase II. PP2A is localized at kinetochores around the centromeric ACA staining, and also between sister centromeres (Fig4A), similar to Sgo2 (Gryaznova *et al*, 2021). Indeed, levels of total PP2A were significantly higher in late than in early metaphase II, and weakly affected by STLC at both cell cycle stages (Fig4A-B). We also confirmed that the pool of PP2A located at kinetochores, which is most likely the one dephosphorylating Hec1, is increased in late metaphase II (Fig4C). We conclude that PP2A accumulates at kinetochores during metaphase II and antagonizes Aurora B/C activity, ultimately stabilizing kinetochore attachments in late metaphase II independently of low tension.

**Incorrect attachments on monopolar spindles can be corrected in early and late metaphase II**

Based on our results, we hypothesized that incorrect attachments can be corrected in early metaphase II but not in late metaphase II. To verify this hypothesis, we artificially created incorrect attachments in early and late metaphase II by using high doses of STLC, producing monopolar spindles. On these monopolar spindles, all sister chromatids are attached to the same pole, and therefore, are under low tension. To determine whether these monopolar attachments can be corrected, oocytes were released from STLC treatment, to allow spindle bipolarization. After STLC removal, the time required for chromosomes to detach, reattach

and align at the metaphase plate was measured by time-lapse microscopy in oocytes expressing H2B-RFP and Tubulin-GFP. We used the timing of chromosome realignment as a read out for error correction efficiency. Of note, similar experiments have been performed in mitosis to study the mechanisms underlying error correction (Lampson *et al*, 2004). If error correction is functional, Aurora B/C should promote destabilization and correction of monopolar attachments, and chromosomes should realign correctly. We expected functional error correction in early but not late metaphase II, where high levels of PP2A were expected to stabilize monopolar attachments. Surprisingly though, after STLC removal, monopolar attached sister chromatids were able to correctly align even more efficiently in late than in early metaphase II (Fig5A; FigS4A; Movie7). This suggests that microtubules were able to detach and establish correct bipolar attachments to sister chromatids even in late metaphase II. Thus, under these experimental conditions, the high levels of PP2A in late metaphase II are not sufficient to stabilize monopolar attachments. One hypothesis is that monopolar spindles may promote more efficient phosphorylation of Aurora B/C targets and error correction. Indeed, it has been shown that Aurora A, localized at spindle poles, can contribute to phosphorylate the same substrates as Aurora B/C on kinetochores that are closer to the poles when sister chromatids are bioriented (Chmátal *et al*, 2015; Ye *et al*, 2015; DeLuca *et al*, 2017). Overall, our data show that the error correction system is still functional in late metaphase II, at least to correct the most severe errors leading to complete loss of tension, such as generated by a monopolar spindle.

**The duration of chromosome alignment is critical for attachment stability**

Although error correction is able to correct monopolar attachments, we have shown that it is not efficient enough to correct bipolar tension-less attachments in late metaphase II, presumably because of high levels of PP2A. We hypothesized that the "age" of the spindle and therefore the “age” of KT-MT attachments, would affect the efficiency of error correction. In this case, KT-MT interactions can be efficiently corrected shortly after sister chromatid biorientation, but not after a longer period, regardless of oocytes being in early or late metaphase II. If this hypothesis is true, de *novo* establishment of KT-MT interactions should allow error correction in late metaphase II, while “old” KT-MT interactions would not. To induce de *novo* KT-MT attachments without using harsh drug treatment such as

nocodazole, late metaphase II oocytes were exposed to a 30 min cold treatment to depolymerize spindles. After depolymerization, oocytes were returned to 37°C to allow spindles to repolymerize. We observed that bipolar spindles reform and chromosomes align within 1 h (FigS4B; Movie8). Next, we compared the effect of reducing tension with STLC, immediately or 6 h after spindle reformation and realignment of chromosomes, in late metaphase II. When STLC was added immediately after chromosome alignment (1 h after return to 37°C), anaphase II was delayed compared to control oocytes (Fig5B, FigS4C, Movie 9). This indicates that shortly after spindle reformation, tension less-attachments are able to induce SAC activation even in late metaphase II. In contrast, when STLC was added 6 h after chromosome alignment (7 h after return to 37°C), anaphase II occurred without delay as in control oocytes (Fig5C, FigS4D, Movie 10). Thus, maintaining chromosome alignment for an extended period in late metaphase II reduces the ability to destabilize attachments in response to low tension, probably due to increasing PP2A accumulation. Indeed, cold treatment decreased PP2A at centromeres and inner centromeres. PP2A staining became more diffuse and displaced around chromosomes (FigS5). After return to 37°C, PP2A is restored at kinetochores within one hour. Overall, our results suggest that the duration of chromosome attachment on the bipolar spindle allows PP2A to accumulate and weaken error correction.

**DISCUSSION**

Meiosis II faces specific challenges such as dealing with segregation errors carried over from meiosis I, or maintaining sister chromatid biorientation for an extended period of time during metaphase II arrest. Thus, the tension-sensing mechanism supposed to detect attachment errors, should be required in meiosis II to prevent post-fertilization aneuploidy. We show here that, once established, inter-KT tension naturally decreases between early and late metaphase II. During metaphase II arrest, chromosomes must remain aligned to the bipolar spindle for hours until fertilization. The time window during which fertilization can take place, before postovulatory aging and oocyte deterioration occur, is quite long (10-12 h post-ovulation in the mouse, and 24 h in human oocytes) (Di Nisio *et al*, 2022; Fissore *et al*, 2002). There is probably no need to maintain high spindle tension throughout the whole length of metaphase II arrest. Instead, relaxing tension in late metaphase II may allow the

oocyte to save energy and may also be important to protect chromosomes from possible breakage due to hard pulling over a long period of time.

As inter-KT tension decreases between early and late metaphase II, it is reasonable that the error correction pathway had to adapt to prevent constant activation, and ongoing destabilization of correct attachments in late metaphase II. Our data demonstrate that SAC functionality is well preserved throughout metaphase II, but that oocytes are only able to correct attachments during a limited temporal window. Tension-less attachments are well detected by the Aurora B/C-dependent error correction pathway in early metaphase II, but escape error correction in late metaphase II. We show that oocytes turn off error correction in late metaphase II by shifting the balance between PP2A and Aurora B/C in favor of PP2A. PP2A-B56 recruitment to kinetochores is mediated by the SAC components BubR1 and Mps1, and we have previously shown that at least Mps1 remains associated with kinetochores in anaphase II (Gryaznova *et al*, 2021), supporting that PP2A is continuously recruited to kinetochores throughout metaphase II arrest. We propose that in late metaphase II, low tension is better tolerated because of the accumulation of more PP2A counteracting Aurora B/C. Consistent with this conclusion, complete spindle depolymerization in late metaphase II resets PP2A levels and allows tension-less attachments to be corrected again on a freshly reformed spindle. Our results also highlight a major difference between meiosis I and meiosis II since low tension allows Aurora B/C to counteract PP2A in metaphase I (Vallot *et al*, 2018), but not in late metaphase II. This could be explained by differences in PP2A levels, which are much higher in metaphase II than in metaphase I (Yoshida et al, 2015). Indeed, PP2A occupies a much larger area in metaphase II arrested oocytes compared to metaphase I. In metaphase II, more than 14 hours after GVBD, PP2A can be found at kinetochores around centromeres, and between sister centromeres, whereas in meiosis I PP2A is only found in between sister centromeres (Chambon *et al*, 2013; Gryaznova *et al*, 2021). We propose that the strong PP2A staining observed in late metaphase II serves mainly to counteract error correction on tension-less, but correct attachments.

As a trade-off, errors that are not repaired early in metaphase II, should persist in late metaphase II. Unexpectedly, late metaphase II oocytes very efficiently converted monopolar

into bipolar attachments, thus demonstrating not only that they are capable of error correction, but also, that they recognize missing tension in the context of a monopolar spindle. Several hypotheses could explain why missing tension is detected on monopolar but not bipolar spindles. The monopolar geometry of sister kinetochores may be more favorable for destabilization of KT-MT interactions by Aurora B/C than the bipolar geometry of sister kinetochores under low tension. Another explanation could be that in the monopolar spindle configuration, attachments are removed by Aurora A-dependent destabilization activity, localized at the poles. Indeed, Aurora A has been shown to locally phosphorylate Hec1 on kinetochores near poles, contributing to destabilize incorrect attachments (Chmátal *et al*, 2015; Ye *et al*, 2015; DeLuca *et al*, 2017). The combined activity of Aurora A at poles and Aurora B/C at kinetochores may be more efficient to counteract PP2A on monopolar spindles, where chromosomes are found closer to the poles. Also, error correction may just become less sensitive with time spent in metaphase II arrest, such that a small reduction of spindle tension is tolerated, but upon gross reduction of tension such as on monopolar spindles, oocytes are still able to detach and reattach microtubules.

Overall, our data using mouse oocytes show a higher susceptibility of late metaphase II oocytes to maintain incorrectly attached chromosomes when efficient fertilization is still possible *in vivo* and *in vitro*. Importantly, in mouse and human oocytes, segregation errors in meiosis II increase with maternal age, due to an increase in misaligned chromosomes, the prevalence of single chromatids, or loss of kinetochore integrity (Shomper *et al*, 2014; Battaglia *et al*, 1996; Zielinska *et al*, 2019; Kouznetsova *et al*, 2022; Webster & Schuh, 2017). Thus, turning off error correction in late metaphase II would have more severe consequences in oocytes from aged mice or older women, since there would be more errors to deal with, and likely more errors persisting until late metaphase II. Importantly, oocytes from aged mice fail to correct aberrant attachments that are under less tension in metaphase II, supporting the inefficiency of error correction (Kouznetsova et al, 2022). Thus, error correction seems to be functional sufficiently long enough for correct segregation in oocytes that are not facing additional challenges, such as increased maternal age for example. Insights into the functionality of error correction relative to the time spent in metaphase II arrest as well as maternal age may contribute to better determine the optimal

temporal window for fertilization in human oocytes to minimize aneuploidies and at the same time, achieve optimal fertilization rates (Chen *et al*, 2023).

## MATERIALS AND METHODS

### Animals

Female CD-1 mice aged 8 weeks were purchased (Janvier, France) and maintained with *ad libitum* access to food and water in the conventional mouse facility of UMR7622 (authorization C75-05-13), IBPS (authorization A75-05-24) and UMR7592 (authorization C75-13-17). The project was approved by an ethical review under French law (authorization B-75-1308). Mice were not exposed to any drug treatment or procedure before being sacrificed by cervical dislocation between 8 and 16 weeks of age.

### Mouse oocyte culture

After dissection of ovaries, oocytes were collected in M2 medium (home-made) supplemented with dibutyryl cyclic AMP at 100 µg/mL (Sigma-Aldrich, D0260) to maintain GV arrest. When necessary, GV-arrested oocytes were injected with specific mRNAs. After several washes in M2 medium without dbcAMP, oocytes undergoing synchronous GVBD within 90 minutes were used for experiments. After GVBD, *in vitro* maturation was performed in drops of M16 medium (home-made or MERK Millipore) covered with mineral oil (FUJIFILM France-Medical Business, 9305) and incubated at 38°C in a CO2 incubator. Experiments were performed in meiosis II after polar body extrusion. Anaphase II can be induced by activating metaphase II arrested oocytes with strontium chloride. In this case, oocytes are incubated in $CaCl_2$-free M2 medium (home-made) for 30-60 min and transferred to $CaCl_2$-free M2 containing 100 mM of strontium chloride (Sigma-Aldrich, 204463).

### Drug treatment

The following drugs were dissolved in DMSO (Sigma-Aldrich, D2650) and were used at the indicated final concentrations in M2 medium: STLC 1 µM or 4 µM (S-Trityl-L-cystein, Sigma-Aldrich, 164739), Nocodazole 0,4 µM (Sigma-Aldrich, M1404), AZD1152-HQPA 0,5 µM (Sigma-Aldrich, SML0268), Reversine 0,5 µM (Interchim, 10004412).

### Fixation of whole oocyte or chromosome spread

The zona pellucida surrounding the oocyte was dissolved in successive drops of Tyrode's acid solution (home-made). Fixation of whole oocytes was performed as described in Vallot et al.

2019. Oocytes were transferred to glass bottom chambers coated with concanavalin A (Sigma-Aldrich) in M2 medium containing PVP (Polyvinylpyrrolidone, Merk Millipore) before slow centrifugation at 1400 rpm for 13 min at 38°C. For spindle staining, oocytes were subjected to cold treatment for 6 min in 80mM Pipes, 1mM MgCl2 in a dish placed on ice. Oocytes were fixed for 30 min in BRB80 buffer containing 0.3% Triton-100X and 1.9% formaldehyde (Sigma-Aldrich F1635). After washes with PBS 1X, oocytes were permeabilized and saturated overnight at 4°C in PBS 1X, 3% BSA, 0.1% Triton-X100. For chromosome spreads, oocytes were fixed in a hypotonic solution (H20, 1% paraformaldehyde (Sigma-Aldrich 441244), 0.15% Triton-X100, 3 mM DTT), which allows the membrane to dissolve and the chromosomes to spread on a 10-well slide (Fischer Scientific-10588681).

**Immunostaining**

After saturation with PBS 1X, 3% BSA, fixed whole oocytes or chromosome spreads were incubated with primary antibodies for 2-3 h, washed and incubated with secondary antibodies for 1h30, at room temperature. The following antibodies were used at the indicated concentrations: Human anti-centromere protein antibody (ACA, Clinisciences, 15-234-0001, 1:100), mouse monoclonal anti- αTubulin conjugated with FITC (DM1A, Sigma-Aldrich, F2168, 1:100), rabbit polyclonal anti-Hec1pS55 (Euromedex, GTX70017, 1:100), rabbit polyclonal anti-Mad2 (1:100) (Wassmann & Benezra, 1998), mouse monoclonal anti-PP2A C-subunit clone 1D6 conjugated with Alexa Fluor 488 (Sigma-Aldrich, 05-421-AF488, 1:50). Anti-human Cy3 (Jackson ImmunoResearch, 709-166-149, 1:200), anti-rabbit AF 488 (Jackson ImmunoResearch, 711-546-152, 1:200), anti-mouse AF488 (Jackson ImmunoResearch, 715-546-150, 1:200). Slides were mounted using VECTASHIELD mounting medium supplemented with DAPI (Eurobio H-1200).

***In vitro* transcription and oocyte microinjection**

H2B-RFP, Securin-YFP or Tubulin-GFP coding sequences inserted into the pRN3 plasmid were used for *in vitro* transcription. Plasmids were digested with SfiI restriction enzyme, and the resulting linearized plasmid was purified by phenol/chloroform purification. *In vitro* transcription was performed by using the mMessage mMachine T3 Kit (Invitrogen, AM1348). After 2 h of transcription, mRNAs were purified by using the RNeasy Mini Kit (Qiagen, 74104).

Purified mRNAs were injected into GV-arrested oocytes using a FemtoJet microinjector pump (Eppendorf) with continuous flow, on an inverted Nikon Eclipse Ti microscope. Microinjection pipettes were made by pulling capillaries (Harvard Apparatus, 30-0038) with a magnetic puller (Narishige, PN-31) and oocytes were manipulated using a holding pipette (Eppendorf, 5178108.000).

**Image acquisition and live imaging**

Chromosome spreads and fixed whole oocytes were observed on an inverted Zeiss Axiovert 200M microscope, coupled to an EMCCD camera (Evolve 512, Photometrics) and a Yokogawa CSU-X1 spinning disc, with a 100X/1.4 NA oil objective. 6-10 Z-sections spaced by 0,4 µm were acquired for chromosome spreads and 25-30 Z-sections spaced by 0,4 µm were acquired for whole oocytes.

Live imaging was performed at 38°C on the same microscope with a 63X/1.4NA oil objective (Figure 1A, and Figure S4A-B) or on a Nikon Eclipse TE2000-E inverted microscope coupled to a PrecisExite High PowerLED fluorescence, a Prime sCMOS camera and a Plan APO 20X/0.75 NA objective (Figure S2, and Figure S4C-D). 15 Z sections spaced by 3 µm were acquired every 10 min. When indicated, chromosomes are stained with SirDNA 1 µM (far-red DNA labelling probe, TEBU BIO, 251SC007) added in the culture medium 1 h prior to imaging.

All Images were acquired with Metamorph software using the same setting for all conditions and replicated experiments. Movies, composites and image projections were generated on Fiji software (NIH). The quantifications have been realized on SUM projections. Brightness and contrast were adjusted equally to all compared conditions.

**Quantification and statistical analysis**

Quantifications were performed by using Fiji software. For quantifications on chromosome spread (Mad2, pS55Hec1, PP2A), a circle of 10x10 pixels was placed around each centromere. Background signal was measured in a second circle placed on chromosome next to the centromeres. The mean fluorescence intensities were measured on sum projections for channels corresponding to the protein of interest and to ACA. After background subtraction, the mean fluorescence intensities were normalized on ACA signals from the same centromere. In figures 4B and S5, the mean fluorescence intensities of PP2A were measured in areas selected manually including centromeres and inner centromere.

Fluorescence intensities were plotted on a graphic by using GraphPad Prism 6 software, and statistical analysis were performed by using nonparametric Mann-Whitney U-test (ns: not significant, * $p< 0.05$, ** $p< 0.001$, *** $p< 0.0001$) and include at least two independent experiments.

For quantification of Securin-YFP on time-lapse, mean fluorescence intensities were measured in a square of 100x100 pixels placed in the oocyte. Background signal was measured in a second square placed outside of the oocyte. Mean intensities were measured on the max projection for each time point of the time-lapse. After background subtraction, the mean fluorescence intensities of Securin-YFP were normalized on the $t_0$ value of the time-lapse.

For quantification of spindle Tubulin on fixed whole oocytes (FigS1F), the integrated densities of tubulin were measured in an ellipse placed around the entire spindle. Background signals were measured in a second ellipse next to the spindle. Integrated densities were measured on sum projections of oocytes before and after a cold treatment for 10 min. After background subtraction, the ratio between integrated density after cold treatment relative to before cold treatment were calculated for each oocyte.

**ACKNOWLEDGEMENTS**

We are grateful to Sandra Touati and Aude Dupré for discussion and comments on the manuscript. We thank Anastasia Shihabi and Maya Merabet for experiments during their undergraduate internships, and members of the MOM group for advices and discussions. AL received a 1-year PhD fellowship from the Labex Who Am I (ANR-11-LABX-0071; Idex ANR-18-IDEX-0001). The KW Lab was funded by the Agence Nationale de la Recherche (ANR-19-CE13-0015), La Fondation de la Recherche Médicale (Equipe FRM DEQ 202103012574) and core funding by the CNRS, Université Paris Cité and Sorbonne Université.

**CONFLICT OF INTEREST**

The authors declare that there is no conflict of interest associated with this study.

**AUTHOR CONTRIBUTIONS**

Experiments were performed by A.L, A.K-S and E.B. Figures were prepared by E.B. The manuscript was written by E.B. with help from K.W. and input from all authors. Funding was obtained by K.W, supervision and project administration were done by E.B. and K.W.

**REFERENCES**


Avo Santos M, Van De Werken C, De Vries M, Jahr H, Vromans MJM, Laven JSE, Fauser BC, Kops GJ, Lens SM & Baart EB (2011) A role for Aurora C in the chromosomal passenger complex during human preimplantation embryo development. *Human Reproduction* 26: 1868–1881

Balboula AZ & Schindler K (2014) Selective disruption of aurora C kinase reveals distinct functions from aurora B kinase during meiosis in mouse oocytes. *PLoS Genet* 10: e1004194

Battaglia DE, Goodwin P, Klein NA & Soules MR (1996) Influence of maternal age on meiotic spindle assembly in oocytes from naturally cycling women. *Hum Reprod* 11: 2217–22

Cairo G, Greiwe C, Jung GI, Blengini C, Schindler K & Lacefield S (2023) Distinct Aurora B pools at the inner centromere and kinetochore have different contributions to meiotic and mitotic chromosome segregation. *Mol Biol Cell* 34: ar43

Chambon JP, Touati SA, Berneau S, Cladière D, Hebras C, Groeme R, McDougall A & Wassmann K (2013) The PP2A inhibitor I2PP2A is essential for sister chromatid segregation in oocyte meiosis II. *Current Biology* 23: 485–490

Charalambous C, Webster A & Schuh M (2023) Aneuploidy in mammalian oocytes and the impact of maternal ageing. *Nat Rev Mol Cell Biol* 24: 27–44

Chen J, Wang Y, Fang C & Li T (2023) A 3–4 h oocyte retrieval-ICSI interval optimizes clinical outcomes for women over 40 years. *Sci Rep* 13: 15035

Chmátal L, Yang K, Schultz RM & Lampson MA (2015) Spatial Regulation of Kinetochore Microtubule Attachments by Destabilization at Spindle Poles in Meiosis i. *Current Biology* 25: 1835–1841

DeLuca JG, Gall WE, Ciferri C, Cimini D, Musacchio A & Salmon ED (2006) Kinetochore Microtubule Dynamics and Attachment Stability Are Regulated by Hec1. *Cell* 127: 969–982

DeLuca KF, Lens SMA & DeLuca JG (2011) Temporal changes in Hec1 phosphorylation control kinetochore-microtubule attachment stability during mitosis. *J Cell Sci* 124: 622–634

DeLuca KF, Meppelink A, Broad AJ, Mick JE, Peersen OB, Pektas S, Lens SMA & DeLuca JG (2017) Aurora A kinase phosphorylates Hec1 to regulate metaphase kinetochore-microtubule dynamics. *J Cell Biol* 217: jcb.201707160

Dumont J & Desai A (2012) Acentrosomal spindle assembly and chromosome segregation during oocyte meiosis. *Trends Cell Biol* 22: 241–9

Dumont J, Petri S, Pellegrin F, Terret ME, Bohnsack MT, Rassinier P, Georget V, Kalab P, Gruss OJ & Verlhac MH (2007) A centriole- and RanGTP-independent spindle assembly pathway in meiosis I of vertebrate oocytes. *Journal of Cell Biology* 176: 295–305

Fissore R, Kurokawa M, Knott J, Zhang M & Smyth J (2002) Mechanisms underlying oocyte activation and postovulatory ageing. *Reproduction*: 745–754

Foley EA, Maldonado M & Kapoor TM (2011) Formation of stable attachments between kinetochores and microtubules depends on the B56-PP2A phosphatase. *Nat Cell Biol* 13: 1265–1271

Gryaznova Y, Keating L, Touati SA, Cladière D, El Yakoubi W, Buffin E & Wassmann K (2021) Kinetochore individualization in meiosis I is required for centromeric cohesin removal in meiosis II. *EMBO J* 40: 1–19

Hassold T & Hunt P (2001) To err (meiotically) is human: the genesis of human aneuploidy. *Nat Rev Genet* 2: 280–91.

Keating L, Touati SA & Wassmann K (2020) A PP2A-B56-Centered View on Metaphase-to-Anaphase Transition in Mouse Oocyte Meiosis I. *Cells* 9: 390
Kitajima TS (2018) Mechanisms of kinetochore-microtubule attachment errors in mammalian oocytes. *Dev Growth Differ* 60: 33–43
Kitajima TS, Ohsugi M & Ellenberg J (2011) Complete kinetochore tracking reveals error-prone homologous chromosome biorientation in mammalian oocytes. *Cell* 146: 568–581
Kouznetsova A, Hernandez-Hernandez A & Hoog C (2014) Merotelic attachments allow alignment and stabilization of chromatids in meiosis II oocytes. *Nat Commun* 5: 4409
Kouznetsova A, Kitajima TS, Brismar H & Höög C (2019) Post-metaphase correction of aberrant kinetochore-microtubule attachments in mammalian eggs. *EMBO Rep* 20
Kouznetsova A, Liu JG, Valentiniene S, Brismar H & Höög C (2022) Age-dependent aneuploidy in mammalian oocytes instigated at the second meiotic division. *Aging Cell* 21
Lampson MA & Cheeseman IM (2011) Sensing centromere tension: Aurora B and the regulation of kinetochore function. *Trends Cell Biol* 21: 133–40
Lampson MA, Renduchitala K, Khodjakov A & Kapoor TM (2004) Correcting improper chromosomes-spindle attachments during cell division. *Nat Cell Biol* 6: 232–237
Liu D, Vader G, Vromans MJM, Lampson MA & Lens SMA (2009) Sensing chromosome bi-orientation by spatial separation of Aurora B kinase from kinetochore substrates. *Science (1979)* 323: 1350–1353
Mailhes JB, Mastromatteo C & Fuseler JW (2004) Transient exposure to the Eg5 kinesin inhibitor monastrol leads to syntelic orientation of chromosomes and aneuploidy in mouse oocytes. *Mutat Res Genet Toxicol Environ Mutagen* 559: 153–167
Maresca TJ & Salmon ED (2009) Intrakinetochore stretch is associated with changes in kinetochore phosphorylation and spindle assembly checkpoint activity. *Journal of Cell Biology* 184: 373–381
McVey SL, Cosby JK & Nannas NJ (2021) Aurora B Tension Sensing Mechanisms in the Kinetochore Ensure Accurate Chromosome Segregation. *Int J Mol Sci* 22: 8818
Mihajlovi AI & Fitzharris G (2018) Current Biology Review Segregating Chromosomes in the Mammalian Oocyte. 895–907
Nagaoka SI & Hassold TJ (2013) Human aneuploidy: mechanisms and new insights into an age- old problem. *Nat Rev Genet* 13: 493–504
Nguyen AL & Schindler K (2017) Specialize and Divide (Twice): Functions of Three Aurora Kinase Homologs in Mammalian Oocyte Meiotic Maturation. *Trends Genet* 33: 349–363
Di Nisio V, Antonouli S, Damdimopoulou P, Salumets A & Cecconi S (2022) In vivo and in vitro postovulatory aging: when time works against oocyte quality? *J Assist Reprod Genet* 39: 905–918
Ozturk S (2022) Molecular determinants of the meiotic arrests in mammalian oocytes at different stages of maturation. *Cell Cycle* 21: 547–571
Petronczki M, Siomos MF, Nasmyth K, Correns C, Vries H De & Tscher- E (2003) Un Me´nage a` Quatre: The Molecular Biology of Chromosome Segregation in Meiosis. 112: 423–440
Schuh M & Ellenberg J (2007) Self-Organization of MTOCs Replaces Centrosome Function during Acentrosomal Spindle Assembly in Live Mouse Oocytes. *Cell* 130: 484–498
Shomper M, Lappa C & FitzHarris G (2014) Kinetochore microtubule establishment is defective in oocytes from aged mice. *Cell Cycle* 13: 1171–1179
Skoufias DA, DeBonis S, Saoudi Y, Lebeau L, Crevel I, Cross R, Wade RH, Hackney D & Kozielski F (2006) S-trityl-L-cysteine is a reversible, tight binding inhibitor of the human

kinesin Eg5 that specifically blocks mitotic progression. *Journal of Biological Chemistry* 281: 17559–17569

Tang A, Shi P, Song A, Zou D, Zhou Y, Gu P, Huang Z, Wang Q, Lin Z & Gao X (2016) PP2A regulates kinetochore-microtubule attachment during meiosis I in oocyte. *Cell Cycle* 15: 1450–1461

Tang CJC, Lin CY & Tang TK (2006) Dynamic localization and functional implications of Aurora-C kinase during male mouse meiosis. *Dev Biol* 290: 398–410

Vallot A, Leontiou I, Cladière D, El Yakoubi W, Bolte S, Buffin E & Wassmann K (2018) Tension-Induced Error Correction and Not Kinetochore Attachment Status Activates the SAC in an Aurora-B/C-Dependent Manner in Oocytes. *Current Biology* 28: 130-139.e3

Wassmann K & Benezra R (1998) Mad2 transiently associates with an APCp55Cdc complex during mitosis

Webster A & Schuh M (2017) Mechanisms of Aneuploidy in Human Eggs. *Trends Cell Biol* 27: 55–68

Welburn JPI, Vleugel M, Liu D, Yates JR, Lampson M a, Fukagawa T & Cheeseman IM (2010) Aurora B Phosphorylates Spatially Distinct Targets to Differentially Regulate the Kinetochore-Microtubule Interface. *Mol Cell* 38: 383–392

Yakoubi W El & Wassmann K (2017) Cell Division Machinery and Disease. 1002: 1–17

Ye AA, Cane S & Maresca TJ (2016) Chromosome biorientation produces hundreds of piconewtons at a metazoan kinetochore. *Nat Commun* 7: 1–9

Ye AA, Deretic J, Hoel CM, Hinman AW, Cimini D, Welburn JP & Maresca TJ (2015) Aurora A Kinase Contributes to a Pole-Based Error Correction Pathway. *Current Biology* 25: 1842–1851

Yoshida S, Kaido M & Kitajima TS (2015) Inherent Instability of Correct Kinetochore-Microtubule Attachments during Meiosis I in Oocytes. *Dev Cell* 33: 589–602

Zielinska AP, Bellou E, Sharma N, Frombach AS, Seres KB, Gruhn JR, Blayney M, Eckel H, Moltrecht R, Elder K, *et al* (2019) Meiotic Kinetochores Fragment into Multiple Lobes upon Cohesin Loss in Aging Eggs. *Current Biology* 29: 3749-3765.e7

## FIGURE LEGENDS

### Figure 1

**Proper chromosome alignment does not correlate with high tension in late metaphase II**

(A) Oocytes injected with H2B-RFP and Tubulin-GFP mRNA were observed by time-lapse microscopy. Hours after Germinal Vesicle Breakdown (GVBD) are indicated. Scale bar: 20 µm.

(B) Timing of anaphase I, polar body extrusion (PBE), interkinesis, and first alignment of chromosomes in each oocyte from panel A. Median is indicated. The red and blue points correspond respectively to the three earliest and the three latest oocytes doing anaphase I. n: number of oocytes.

(C) Meiosis II oocytes were fixed at 12h, 14h, 16h or 18h after GVBD and stained with DAPI (blue) and anti-Tubulin antibody (green). Scale bar: 20 µm. Arrows indicate unaligned chromosomes.

(D) Percentage of oocytes containing 0, 1-2, or more than 2 unaligned chromosomes in the oocytes from panel C. n: number of oocytes.

(E) Magnification of sister chromatids stained with DAPI (blue), ACA (red) and anti-Tubulin antibody (green). Scale bar: 5 µm. The scheme represents two sister chromatids (blue), centromeres (red), and microtubule fibres (green). The double-headed arrows indicate inter-kinetochore distance.

(F) Inter-kinetochore (inter-KT) distances (µm) were measured in oocytes from panel C as indicated in E. Median and interquartile range are indicated. n: number of sister chromatid pairs.

Each graph includes the values of at least 3 independent experiments and p values have been calculated by using Mann-Whitney's test (*** $p<0.0001$; ns: not significant).

### Figure 2

**Only in early metaphase II oocytes recognize missing tension in an Aurora B/C- and SAC-dependent manner**

(A) Scheme of the experimental settings in the panels (B-G) below: oocytes were injected in GV (Germinal Vesicle) stage with the indicated mRNAs, released and re-synchronised at GVBD (Germinal Vesicle Breakdown). Meiosis II oocytes were submitted to drug treatment

as indicated, at 12h or 18h after GVBD. Then, oocytes were activated by addition of strontium (Str) and their ability to progress in anaphase II was analysed by time-lapse imaging.

(B) Oocytes injected with Securin-YFP mRNA were left untreated (Ctrl) or treated with nocodazole (Noc) for 1 h at GVBD+12h or GVBD+18h. After addition of strontium, the level of Securin-YFP was measured in each oocyte for each time point of the time-lapse. n: number of oocytes.

(C) Meiosis II oocytes were left untreated (Ctrl) or treated with Nocodazole (Noc) or STLC for 1 h, at GVBD+12h or GVBD+18h. Chromosomes were spread and stained with ACA (red), anti-Mad2 antibody (green) and DAPI (blue). Small images correspond to magnification of chromosomes. Scale bars: 10 µm. n: number of oocytes.

(D) The mean intensity of Mad2 signal per centromere from (C) has been quantified and normalized on the mean intensity of ACA (AU: arbitrary unit). The values from 2 independent experiments are shown and median and interquartile range are indicated. p values have been calculated by using Mann-Whitney's test (*** $p<0.0001$). n: number of centromeres.

(E) Oocytes injected with H2B-RFP mRNA were left untreated (Ctrl) or treated with STLC and/or reversine (Rev) at GVBD+12h for 1 h. After addition of strontium, the percentage of oocytes undergoing anaphase II relative to time after activation was determined by time-lapse microscopy. n: number of oocytes.

(F) Oocytes injected with Securin-YFP were left untreated (Ctrl) or treated with STLC alone, AZD1152 (AZD) alone, or with both STLC and AZD, at GVBD+12h for 1 h. After addition of strontium, the level of Securin-YFP was measured in each oocyte for each time point of the time-lapse. n: number of oocytes.

(G) Oocytes injected with H2B-RFP mRNA were left untreated (Ctrl) or treated with STLC at GVBD+12h or GVBD+18h for 1 h. After addition of strontium, the percentage of oocytes undergoing anaphase II relative to time after activation was determined by time-lapse microscopy. n: number of oocytes.

**Figure 3**

**Low tension induces more Hec1 phosphorylation in early than in late metaphase II**

(A) Meiosis II oocytes at 12h or 18h after GVBD were treated with STLC for 1 h where indicated, and chromosomes were spread and stained with ACA (red), anti-phosphoS55

Hec1 antibody (pHec1; green) and DAPI (blue). Small images correspond to magnification of chromosomes. Scale bar: 10 µm. n is the number of oocytes.

(B) The mean intensity of pS55 Hec1 signal per centromere has been quantified and normalized to the mean intensity of ACA (AU: arbitrary unit). n is the number of centromeres analyzed from 3 independent experiments. Median and interquartile range are indicated. p values have been calculated by using Mann-Whitney's test (*** $p<0.0001$, ns: not significant).

**Figure 4**

**Centromeric PP2A accumulates to higher levels as oocytes progress into late metaphase II**

(A) Meiosis II oocytes at 12h or 18h after GVBD were treated with STLC for 1 h where indicated, and chromosomes were spread and stained with ACA (red), anti-PP2A antibody (green) and DAPI (blue). Small images correspond to magnification of chromosomes. Scale bar: 10 µm. n is the number of oocytes.

(B) The mean intensity of total PP2A signal including centromeres and inner centromeres has been quantified and normalized to the mean intensity of ACA (AU: arbitrary unit). n is the number of centromere pairs analyzed from 3 independent experiments. Median and interquartile range are indicated. p values have been calculated by using Mann-Whitney's test (*** $p<0.0001$, *$p<0,05$, ns: not significant).

(C) The mean intensity of centromeric PP2A signal (overlapping with ACA staining) has been quantified and normalized to the mean intensity of ACA (AU: arbitrary unit). n is the number of centromeres analyzed from 3 independent experiments. Median and interquartile range are indicated. p values have been calculated by using Mann-Whitney's test (*** $p<0.0001$, ns: not significant).

**Figure 5**

**Age of the bipolar spindle determines error correction efficiency**

In (A) (B) (C), the scheme in the left illustrates the experimental protocol of the experiment.

(A) Oocytes were injected with H2B-RFP and Tubulin-GFP mRNAs at GV stage, and treated with elevated concentrations of STLC (4µM) at GVBD+12h or GVBD+18h to induce monopolar spindles. After 1 h, oocytes were washed to remove STLC. Bipolarization of the spindle and realignment of chromosomes were followed by time-lapse microscopy. On the

right, the time required for chromosome alignment after wash-out was quantified for each oocyte. n is the number of oocytes analyzed from 2 independent experiments. Median and interquartile range are indicated. p values have been calculated by using Mann-Whitney's test (** $p<0.001$).

(B-C) Oocytes were submitted to a cold treatment for 30 min in order to depolymerize spindles at GVBD+18h. Then, oocytes were incubated at 37°C in order to allow spindle repolymerization and chromosome realignment. After 1 h at 37°C in (B) or after 7 h at 37°C in (C), oocytes were treated with STLC for 1 h where indicated, and chromosomes were stained with SirDNA. After activation by addition of strontium, chromosome segregation was followed by time-lapse microscopy. On the right, the graphs represent the cumulative percentage of oocytes entering anaphase II relative to time after strontium addition for each condition. n is the number of oocytes analyzed from 3 independent experiments.

## SUPPLEMENTAL FIGURE LEGENDS

### Figure S1

**During metaphase II, chromosomes progressively align and the spindle becomes more stable**

(A) Meiosis II oocytes were fixed without pre-cold treatment at 12h or 18h after GVBD and stained with DAPI (blue) and anti-Tubulin antibody (green). Scale bar: 20 µm. (B) Percentage of oocytes containing 0, 1-2, or more than 2 unaligned chromosomes in oocytes from panel A. n: number of oocytes analysed in 1 representative experiment.

(C) Representative spindle image from figure 1C. The rectangle defines the metaphase plate and the double-headed arrow indicates how the metaphase plate width has been measured.

(D) Metaphase plate width measured in each oocyte. Median and interquartile range are indicated. n is the number of oocytes analyzed from at least 3 independent experiments for each condition. p values have been calculated by using Mann-Whitney's test (*** $p<0.0001$, *$p<0.05$, ns: not significant).

(E) Live oocytes previously injected with H2B-RFP and Tubulin-GFP mRNA were observed at 12h or 18h after GVBD, before and after a cold treatment of 10 min. Scale bar: 20 µm. (F) Tubulin density per spindle has been quantified before and after cold treatment in the same oocyte. The ratios of Tubulin after/before cold treatment for each oocyte are represented in

the graph. Median and interquartile range are indicated. n is the number of oocytes analyzed from 3 independent experiments. p values have been calculated by using Mann-Whitney's test (*** p<0.0001).

**Figure S2**

**Nocodazole and STLC delay anaphase II onset, but the latter only in early metaphase II**

Montage of representative movies analyzed in Figure 2. The time after addition of strontium is indicated (h: min). Arrows indicate sister chromatid segregation and thus, anaphase II onset.

(A) Oocytes injected with Securin-YFP mRNA were left untreated (Ctrl), or treated at GVBD+12h with nocodazole (Noc) for 1 h, and activated by addition of strontium.

(B) Oocytes injected with Securin-YFP mRNA were left untreated (Ctrl) or treated at GVBD+18h with nocodazole (Noc) for 1 h and activated by addition of strontium.

(C) Oocytes injected with H2B-RFP mRNA were left untreated (Ctrl) or treated at GVBD+12h with STLC, +/- Reversine (Rev) for 1 h, and activated by addition of strontium.

(D) Oocytes injected with Securin-YFP mRNA were left untreated (Ctrl), or treated at GVBD+12h with STLC +/- AZD1152 (AZD) for 1 h, and activated by addition of strontium.

(E) Oocytes injected with H2B-RFP mRNA were left untreated (Ctrl) or treated at GVBD+18h with STLC for 1 h, and activated by addition of strontium.

**Figure S3**

**Inhibiting Eg5 induces short spindle and low tension in meiosis II**

(A-B) Meiosis II oocytes at 12h after GVBD (early metaphase II) were left untreated (Ctrl) or treated with STLC for 1 h, fixed and stained with DAPI (blue), anti-Tubulin antibody (green) and ACA (red). (A) The double-headed arrow indicates the spindle length. Scale bar: 20 µm. The graph shows the spindle length measured in each oocyte. Median and interquartile range are indicated. n: number of oocytes. (B) Magnifications on sister chromatid pairs of oocytes from A. The double-headed arrow indicates the inter-kinetochore distance. Scale bar: 5 µm. The graph shows inter-kinetochore (inter-KT) distances measured in each oocyte. Median and interquartile range are indicated. n: number of sister chromatid pairs.

(C-D) Meiosis II oocytes at 18h after GVBD (late metaphase II) were left untreated (Ctrl) or treated with STLC for 1 h, fixed and stained with DAPI (blue), anti-Tubulin antibody (green)

and ACA (red). (C) The double-headed arrow indicates the spindle length. Scale bar: 20 µm. The graph shows the spindle length measured in each oocyte. Median and interquartile range are indicated. n: number of oocytes. (D) Magnifications on sister chromatid pairs of oocytes from C. The double headed-arrow indicates the inter-kinetochore distance. Scale bar: 5 µm. The graph shows inter-kinetochore (inter-KT) distances measured in each oocyte. Median and interquartile range are indicated. n: number of sister chromatid pairs.

Each graph includes the values of at least 3 independent experiments for each condition and p values have been calculated by using Mann-Whitney's test (*** $p<0.0001$; ns: not significant).

**Figure S4**

**Age of the bipolar spindle determines error correction efficiency**

Montage of representative movies analyzed in Figure 5.

(A) Oocytes were injected with H2B-RFP and Tubulin-GFP mRNAs in GV stage, treated with STLC (4 µM) at GVBD+12h or GVBD+18h and washed to remove STLC. Movies were started immediately after wash-out, and time after wash-out is indicated. Bipolarization of the spindle and chromosome realignment (arrow) can be seen.

(B) Oocytes were injected with H2B-RFP and tubulin-GFP mRNAs in GV stage and incubated at 4°C for 30 min at GVBD+18h. Movies were started when oocytes were transferred to 37°C. Repolymerization of the spindle after depolymerization induced by cold treatment can be seen.

(C) Oocytes were incubated at 4°C for 30 min at GVBD+18h and transferred to 37°C for 1 h. Oocytes were treated with STLC for 1 h where indicated and chromosomes were stained with SirDNA before activation by addition of strontium. Movies were started after addition of strontium. Chromosome segregation can be seen (arrows).

(D) Oocytes were incubated at 4°C for 30 min at GVBD+18h and transferred to 37°C for 7 h. Oocytes were treated with STLC for 1 h where indicated and chromosomes were stained with SirDNA before activation by addition of strontium. Movies were started after addition of strontium. Chromosome segregation can be seen (arrows).

**Figure S5**

**PP2A levels reset after spindle depolymerization**

(A) Meiosis II oocytes at 18h after GVBD were cultured at 37°C (Ctrl), 4 °C for 30 min (after Cold), 1h at 37°C after 30 min at 4°C (1h after back to 37°C). Chromosomes were spread and stained with ACA (red), anti-PP2A antibody (green) and DAPI (blue). Small images correspond to magnification of chromosomes. Scale bar: 10 µm. n is the number of oocytes.

(B) The mean intensities of total PP2A signal including centromeres and inner centromeres have been quantified and normalized on the mean intensities of ACA (AU: arbitrary unit). n is the number of centromere pairs analyzed from 2 independent experiments. Median and interquartile range are indicated. p values have been calculated by using Mann-Whitney's test (*** $p<0.0001$, ns: not significant).

## SUPPLEMENTAL MOVIE LEGENDS

**Movie1**

**Progression from metaphase I to metaphase II in control oocyte**

Oocytes were injected with H2B-RFP and Tubulin-GFP mRNA at GV stage. Acquisitions of RFP and GFP channels were started at GVBD+6h (h:min) every 15 min. Shown is the overlay from a stack of 15 z-sections spaced by 3 µm of a representative movie from 23 oocytes obtained from 3 independent experiments (see Fig.1A).

**Movie2**

**Visualization of Securin-YFP after activation in control and nocodazole treated oocytes in early metaphase II**

Oocytes injected with Securin-YFP mRNA at GV stage were left untreated (Ctrl) or treated with Nocodazole (Noc) at GVBD+12h. Acquisitions in the YFP channel were started 20 min after activation by addition of strontium (GVBD+13h), with time points every 10 min (h: min). Shown are overlays from stacks of 15 z-sections spaced by 3 µm of representative

movies from 20 control and 17 nocodazole treated oocytes obtained from at least 3 independent experiments (see Fig2B and S2A).

**Movie3**

**Visualization of Securin-YFP after activation in control and nocodazole-treated oocytes in late metaphase II**

Oocytes injected with Securin-YFP mRNA at GV stage were left untreated (Ctrl) or treated with Nocodazole (Noc), at GVBD+18h. Acquisitions in the YFP channel were started 20 min after activation by addition of strontium (GVBD+19h), with time points every 10 min (h: min). Shown are overlays from stacks of 15 z-sections spaced by 3 µm of representative movies from 16 control and 10 nocodazole treated oocytes obtained from at least 3 independent experiments (see Fig2B and S2B).

**Movie4**

**Visualization of anaphase II after activation in control, STLC, and Reversine+STLC treated oocytes in early metaphase II**

Oocytes injected with H2B-RFP mRNA at GV stage were left untreated (Ctrl) or treated with STLC or Reversine+STLC, at GVBD+12h. Acquisitions in the RFP channel were started 20 min after activation by addition of strontium (GVBD+13h), with time points every 10 min (h: min). Shown are overlays from stacks of 15 z-sections spaced by 3 µm of representative movies from 35 control, 26 STLC and 37 Reversine+STLC treated oocytes obtained from at least 3 independent experiments (see Fig2E and S2C).

**Movie5**

**Visualization of Securin-YFP after activation in control, STLC, and AZD+STLC treated oocytes in early metaphase II**

Oocytes injected with Securin-YFP mRNA at GV stage were left untreated (Ctrl) or treated with STLC, or AZD+Reversine at GVBD+12h. Acquisitions in the YFP channel were started 20 min after activation by addition of strontium (GVBD+13h), with time points every 10 min (h: min). Shown are overlays from stacks of 15 z-sections spaced by 3 µm of representative movies from 17 control, 13 STLC, and 17 AZD+STLC treated oocytes obtained from at least 3 independent experiments (see Fig2F and S2D).

**Movie6**

**Visualization of anaphase II after activation in control and STLC-treated oocytes in late metaphase II**

Oocytes injected with H2B-RFP mRNA at GV stage were left untreated (Ctrl) or treated with STLC at GVBD+18h. Acquisitions in the RFP channel were started 20 min after activation by addition of strontium (GVBD+19h), with time points every 10 min (h: min). Shown are overlays from stacks of 15 z-sections spaced by 3 µm of representative movies from 41 control, 46 STLC treated oocytes obtained from at least 3 independent experiments (see Fig2G and S2E).

**Movie7**

**Visualization of spindle bipolarization after STLC wash-out in early and late metaphase II**

Oocytes injected with H2B-RFP and Tubulin-GFP mRNA at GV stage were treated with STLC at 4 µM at GVBD+12h (top) or GVBD+18h (bottom) for 1 h and washed to remove STLC. Acquisitions of RFP and GFP channels were started 20 min after wash-out, with time points every 10 min (h: min). Shown are overlays from stacks of 15 z-sections spaced by 3 µm of representative movies from 23 early and 15 late metaphase II oocytes obtained from 2 independent experiments (see Fig5A and S4A).

**Movie8**

**Visualization of spindle reformation after cold treatment in late metaphase II**

Oocytes injected with H2B-RFP and Tubulin-GFP mRNA at GV stage were submitted to cold treatment at GVBD+18h for 30 min and returned to 37°C. Acquisitions of RFP and GFP channels were started 10 min after return to 37°C, with time points every 10 min (h: min). Shown are overlays from stacks of 15 z-sections spaced by 3 µm of representative movies from 23 early and 15 late metaphase II oocytes obtained from 2 independent experiments (see Fig5B and S4B).

**Movie9**

**Visualization of anaphase II after activation in control and STLC treated oocytes, 1 after spindle reformation in late metaphase II**

Oocytes were submitted to cold treatment at GVBD+18h for 30 min and returned to 37°C. 1h after return to 37°C, oocytes were left untreated (Ctrl) or treated with STLC for 1 h. Oocytes were incubated with SirDNA to visualize chromosomes and activated with strontium. Acquisitions of RFP and GFP channels were started 20 min after activation, with time points every 10 min (h: min). Shown are overlays from stacks of 15 z-sections spaced by 3 µm, of representative movies from 39 control and 33 STLC treated oocytes obtained from 3 independent experiments (see Fig5B and S4C).

**Movie10**

**Visualization of anaphase II after activation in control and STLC treated oocytes 7h after newly spindle formation in late metaphase II**

Oocytes were submitted to cold treatment at GVBD+18h for 30 min and returned to 37°C. 7h after return to 37°C, oocytes were left untreated (Ctrl) or treated with STLC for 1 h. Oocytes were incubated with SirDNA to visualize chromosomes and activated with strontium. Acquisitions of RFP and GFP channels were started 20 min after activation, with time points every 10 min (h: min). Shown are overlays from stacks of 15 z-sections spaced by 3 µm of representative movies from 31 control and 30 STLC treated oocytes obtained from 3 independent experiments (see Fig5C and S4D).

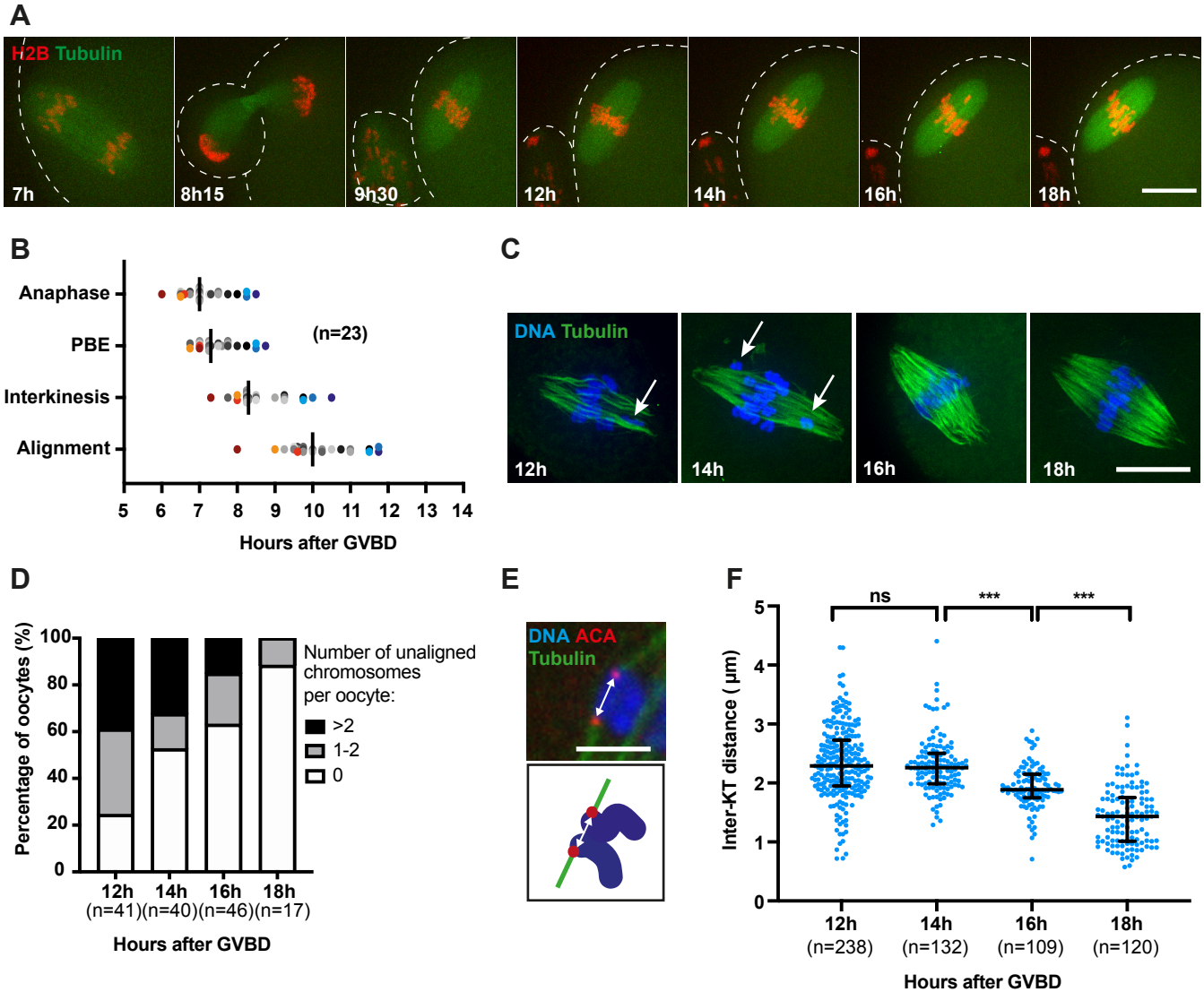
A
H2B Tubulin
7h
8h15
9h30
12h
14h
16h
18h
B
Anaphase
PBE
Interkinesis
Alignment
(n=23)
5 6 7 8 9 10 11 12 13 14
Hours after GVBD
C
DNA Tubulin
12h
14h
16h
18h
D
Percentage of oocytes (%)
100
80
60
40
20
0
Number of unaligned chromosomes per oocyte:
>2
1-2
0
12h (n=41)
14h (n=40)
16h (n=46)
18h (n=17)
Hours after GVBD
E
DNA ACA Tubulin
F
Inter-KT distance (µm)
ns
***
***
5
4
3
2
1
0
12h (n=238)
14h (n=132)
16h (n=109)
18h (n=120)
Hours after GVBD

FIGURE 1

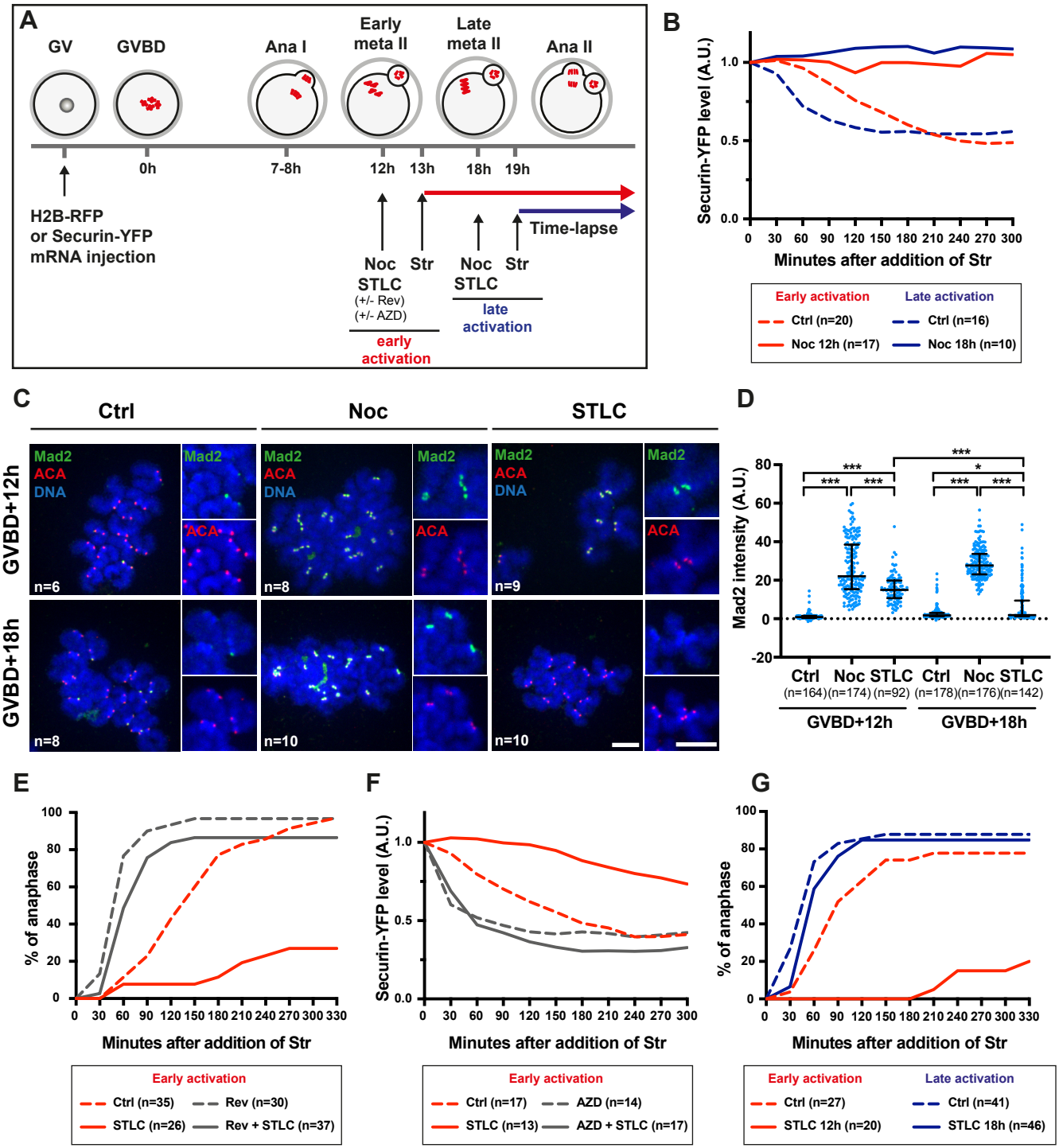
A
GV
GVBD
Ana I
Early meta II
Late meta II
Ana II
0h
7-8h
12h
13h
18h
19h
H2B-RFP
or Securin-YFP
mRNA injection
Time-lapse
Noc
STLC
(+/- Rev)
(+/- AZD)
Str
Noc
STLC
Str
early activation
late activation
B
Securin-YFP level (A.U.)
Minutes after addition of Str
Early activation
Ctrl (n=20)
Noc 12h (n=17)
Late activation
Ctrl (n=16)
Noc 18h (n=10)
C
Ctrl
Noc
STLC
GVBD+12h
GVBD+18h
Mad2
ACA
DNA
n=6
n=8
n=9
n=8
n=10
n=10
D
Mad2 intensity (A.U.)
Ctrl
Noc
STLC
Ctrl
Noc
STLC
(n=164)(n=174)(n=92)
(n=178)(n=176)(n=142)
GVBD+12h
GVBD+18h
E
% of anaphase
Minutes after addition of Str
Early activation
Ctrl (n=35)
Rev (n=30)
STLC (n=26)
Rev + STLC (n=37)
F
Securin-YFP level (A.U.)
Minutes after addition of Str
Early activation
Ctrl (n=17)
AZD (n=14)
STLC (n=13)
AZD + STLC (n=17)
G
% of anaphase
Minutes after addition of Str
Early activation
Ctrl (n=27)
STLC 12h (n=20)
Late activation
Ctrl (n=41)
STLC 18h (n=46)

FIGURE 2

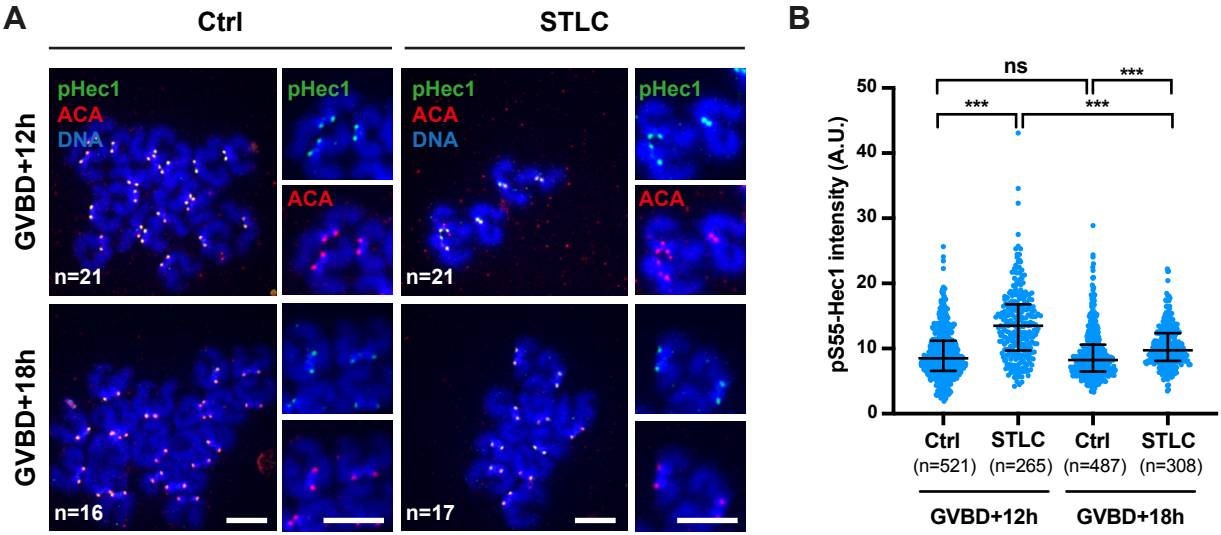
A
Ctrl
STLC
GVBD+12h
GVBD+18h
pHec1
ACA
DNA
n=21
n=21
n=16
n=17
B
pS55-Hec1 intensity (A.U.)
50
40
30
20
10
0
ns
***
***
***
Ctrl
(n=521)
STLC
(n=265)
Ctrl
(n=487)
STLC
(n=308)
GVBD+12h
GVBD+18h

FIGURE 3

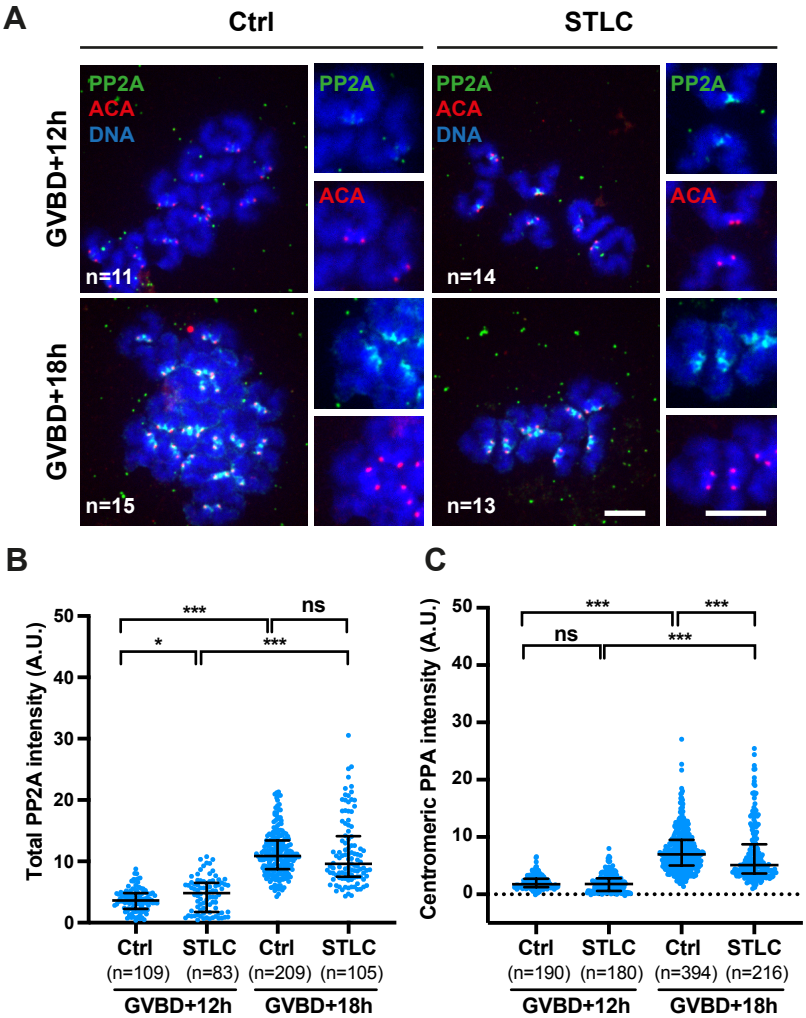
A
Ctrl
STLC
GVBD+12h
GVBD+18h
PP2A
ACA
DNA
n=11
n=14
n=15
n=13
B
Total PP2A intensity (A.U.)
50
40
30
20
10
0
***
ns
*
***
Ctrl
STLC
Ctrl
STLC
(n=109)
(n=83)
(n=209)
(n=105)
GVBD+12h
GVBD+18h
C
Centromeric PPA intensity (A.U.)
50
40
30
20
10
0
***
***
ns
***
Ctrl
STLC
Ctrl
STLC
(n=190)
(n=180)
(n=394)
(n=216)
GVBD+12h
GVBD+18h

FIGURE 4

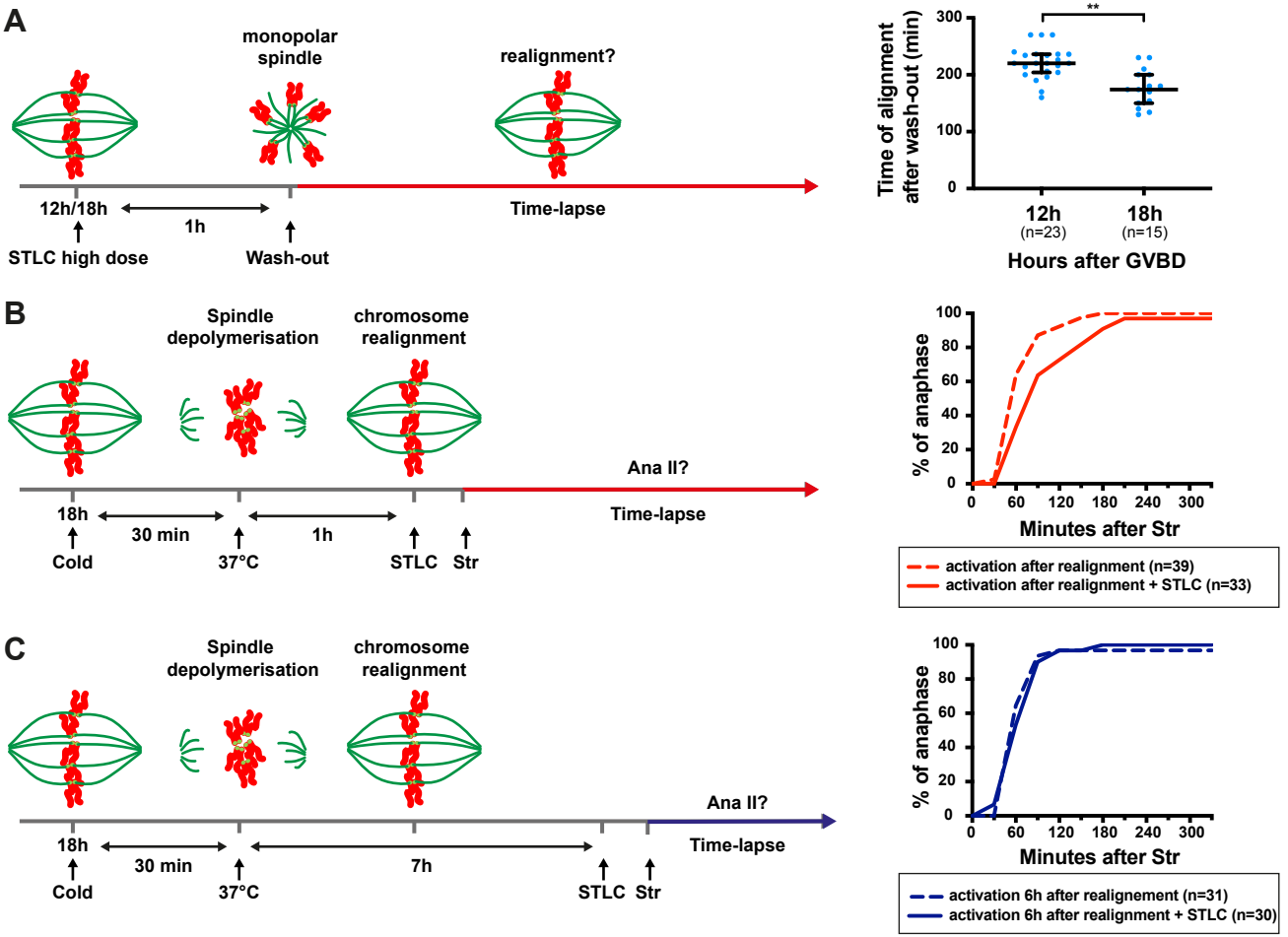
A
monopolar spindle
realignment?
12h/18h
1h
Time-lapse
STLC high dose
Wash-out
Time of alignment after wash-out (min)
**
12h (n=23)
18h (n=15)
Hours after GVBD
B
Spindle depolymerisation
chromosome realignment
Ana II?
18h
30 min
1h
Time-lapse
Cold
37°C
STLC
Str
% of anaphase
Minutes after Str
activation after realignment (n=39)
activation after realignment + STLC (n=33)
C
Spindle depolymerisation
chromosome realignment
Ana II?
18h
30 min
7h
Time-lapse
Cold
37°C
STLC
Str
% of anaphase
Minutes after Str
activation 6h after realignement (n=31)
activation 6h after realignment + STLC (n=30)

# FIGURE 5

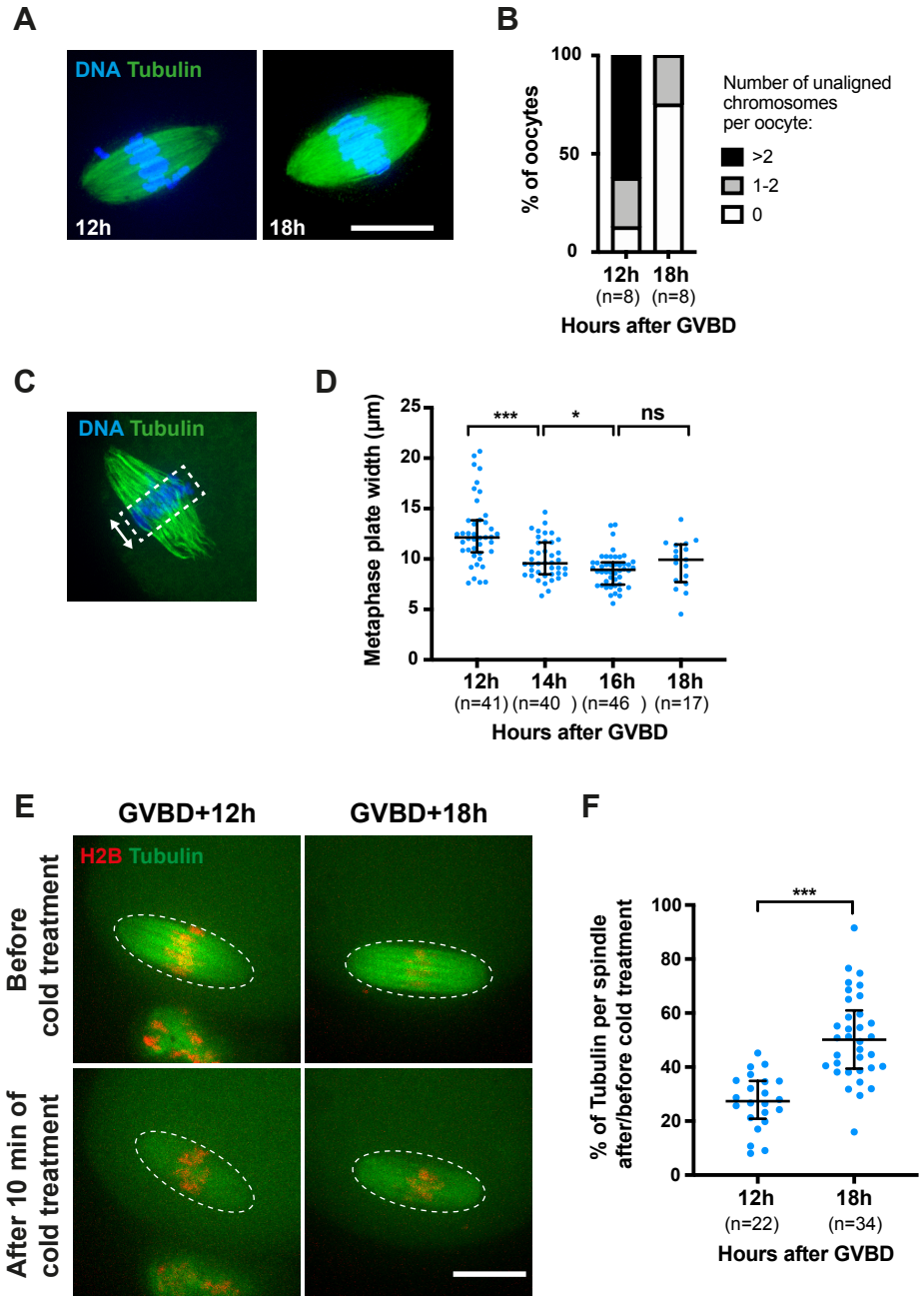
A
DNA Tubulin
12h
18h
B
100
50
0
% of oocytes
Number of unaligned chromosomes per oocyte:
>2
1-2
0
12h (n=8)
18h (n=8)
Hours after GVBD
C
DNA Tubulin
D
Metaphase plate width (µm)
25
20
15
10
5
0
***
*
ns
12h (n=41)
14h (n=40 )
16h (n=46 )
18h (n=17)
Hours after GVBD
E
GVBD+12h
GVBD+18h
H2B Tubulin
Before cold treatment
After 10 min of cold treatment
F
% of Tubulin per spindle after/before cold treatment
100
80
60
40
20
0
***
12h (n=22)
18h (n=34)
Hours after GVBD

FIGURE S1

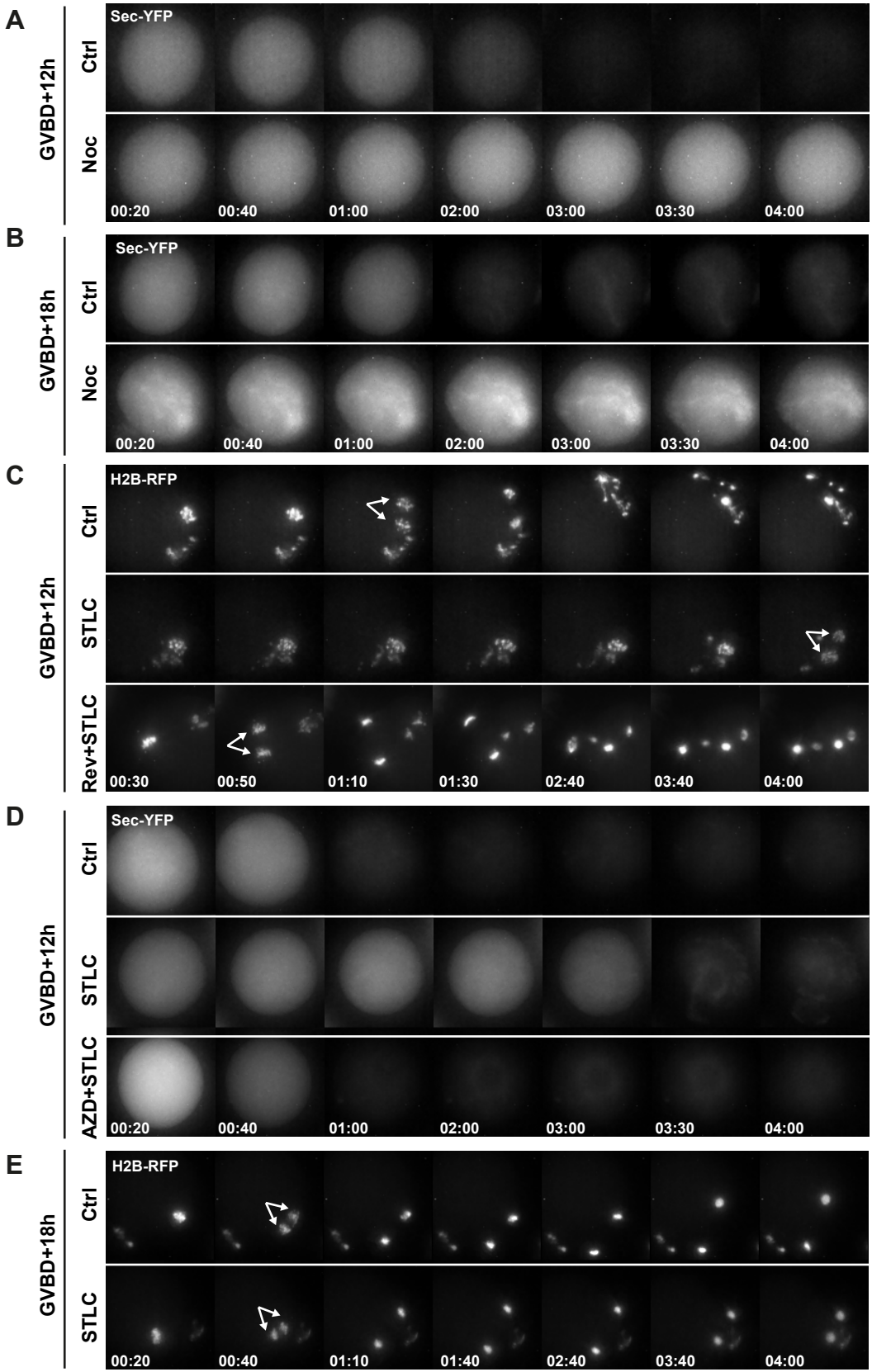
A
GVBD+12h
Ctrl
Noc
Sec-YFP
00:20
00:40
01:00
02:00
03:00
03:30
04:00
B
GVBD+18h
Ctrl
Noc
Sec-YFP
00:20
00:40
01:00
02:00
03:00
03:30
04:00
C
GVBD+12h
Ctrl
STLC
Rev+STLC
H2B-RFP
00:30
00:50
01:10
01:30
02:40
03:40
04:00
D
GVBD+12h
Ctrl
STLC
AZD+STLC
Sec-YFP
00:20
00:40
01:00
02:00
03:00
03:30
04:00
E
GVBD+18h
Ctrl
STLC
H2B-RFP
00:20
00:40
01:10
01:40
02:40
03:40
04:00

FIGURE S2

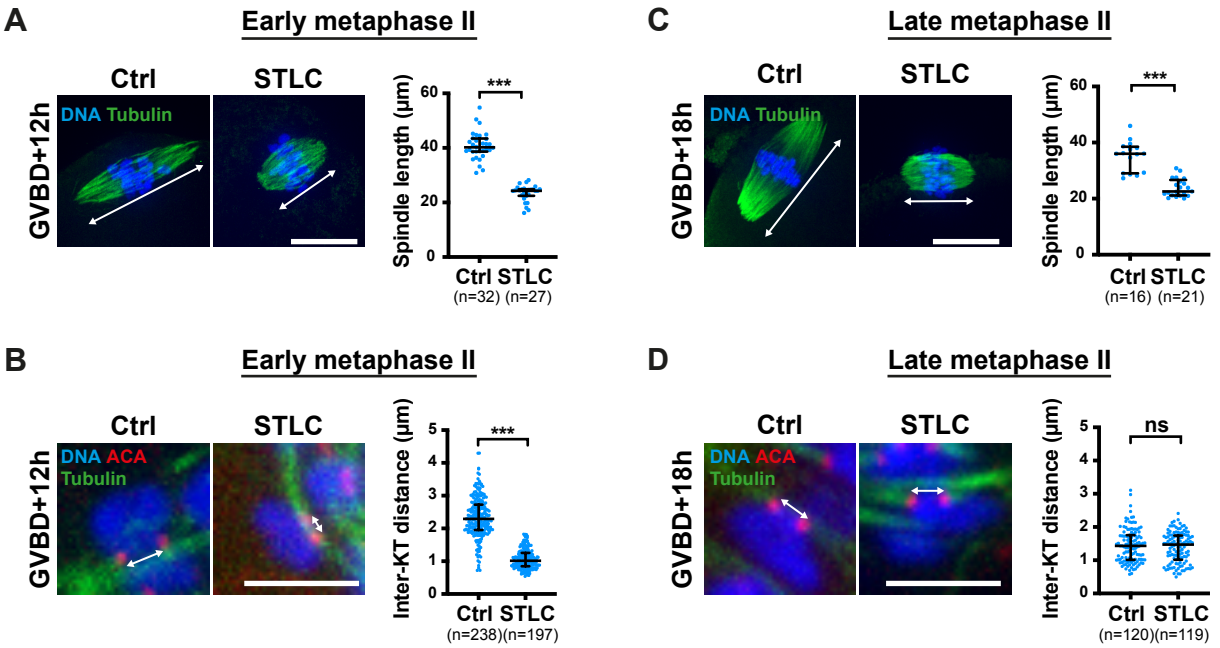
A
Early metaphase II
Ctrl
STLC
GVBD+12h
DNA Tubulin
Spindle length (µm)
***
Ctrl STLC
(n=32) (n=27)
C
Late metaphase II
Ctrl
STLC
GVBD+18h
DNA Tubulin
Spindle length (µm)
***
Ctrl STLC
(n=16) (n=21)
B
Early metaphase II
Ctrl
STLC
GVBD+12h
DNA ACA
Tubulin
Inter-KT distance (µm)
***
Ctrl STLC
(n=238)(n=197)
D
Late metaphase II
Ctrl
STLC
GVBD+18h
DNA ACA
Tubulin
Inter-KT distance (µm)
ns
Ctrl STLC
(n=120)(n=119)

**FIGURE S3**

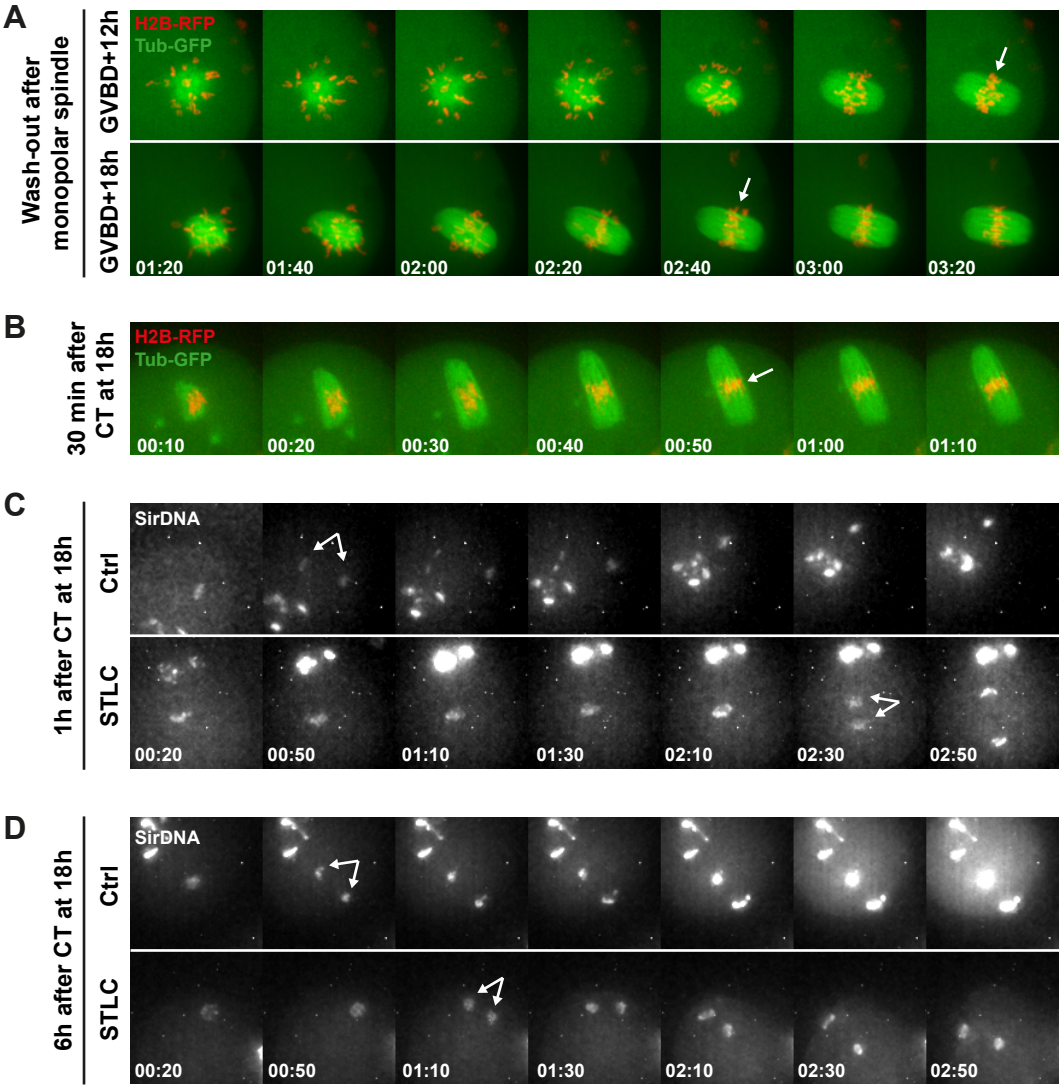
A
Wash-out after monopolar spindle
GVBD+12h
GVBD+18h
H2B-RFP
Tub-GFP
01:20
01:40
02:00
02:20
02:40
03:00
03:20
B
30 min after CT at 18h
H2B-RFP
Tub-GFP
00:10
00:20
00:30
00:40
00:50
01:00
01:10
C
1h after CT at 18h
Ctrl
STLC
SirDNA
00:20
00:50
01:10
01:30
02:10
02:30
02:50
D
6h after CT at 18h
Ctrl
STLC
SirDNA
00:20
00:50
01:10
01:30
02:10
02:30
02:50

FIGURE S4

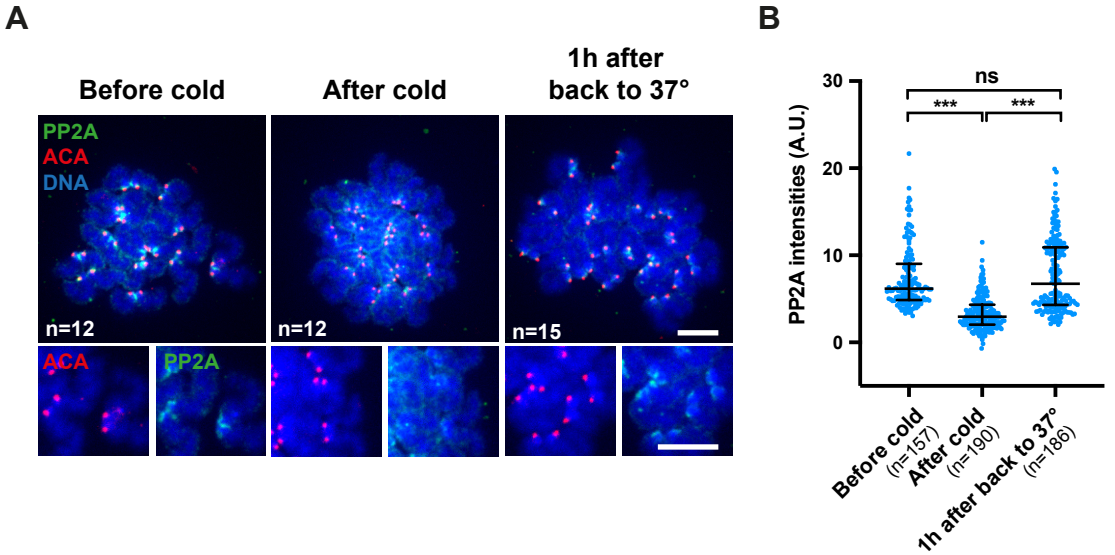
A
Before cold
After cold
1h after back to 37°
PP2A
ACA
DNA
n=12
n=12
n=15
ACA
PP2A
B
ns
***
***
PP2A intensities (A.U.)
30
20
10
0
Before cold (n=157)
After cold (n=190)
1h after back to 37° (n=186)

# FIGURE S5